



# Vortex shedding patterns past a rectangular cylinder near a free surface

Wenjie Zhong<sup>a</sup>, Solomon C. Yim<sup>b</sup>, Lu Deng<sup>a,c,\*</sup>

<sup>a</sup> College of Civil Engineering, Hunan University, Changsha, 410082, Hunan, China

<sup>b</sup> School of Civil and Construction Engineering, Oregon State University, Corvallis, 97331, Oregon State, USA

<sup>c</sup> Key Laboratory for Damage Diagnosis of Engineering Structures of Hunan Province, Changsha, 410082, Hunan, China

## ARTICLE INFO

### Keywords:

Rectangular cylinder  
Free surface  
RANS simulation  
Vortex shedding  
Wakes

## ABSTRACT

The effects of asymmetric boundary conditions on the flow past rectangular cylinders are relevant for many engineering applications. Pertinently, the influence of wall proximity on the flow around cylinders has been widely investigated, and the flow regimes depending on the distance to the wall have been identified. However, a comprehensive study of the flow around rectangular cylinders near a free surface is lacking. The classifications of the flow have not been tackled and the connection between the flow behaviors and the force variations with the depth has not been demonstrated. In this study, multiphase simulations over a broad range of depth-to-length ratios (0.3–4.5) and width-to-length ratios (0.7–5.0) were conducted. Flow results show that the anti-symmetric vortex shedding becomes asymmetric and then suppressed as the depth decreases. Three patterns of asymmetric flow depending on the width-to-length ratio were observed: “asymmetrically separated”, “one-sidedly reattached” and “asymmetrically reattached”. The force variations with the depth for rectangular cylinders with  $0.7 < w/l < 1.5$ ,  $1.5 \leq w/l < 2.8$  and  $2.8 < w/l \leq 5.0$  show different trends due to the occurrence of different asymmetric flows. The boundaries between different flow patterns were defined based on the force variations.

## 1. Introduction

Flow past rectangular cylinders is one of classical problems in fluid mechanics. Extensive investigations on the unbounded flow past rectangular cylinders have been conducted due to its practical importance in engineering applications and scientific significance in fluid mechanics (Mannini et al., 2010; Norberg, 1993; Okajima, 1982; Schewe, 2013). Recently, research on the flow past rectangular cylinders has been extended to incorporate the effects of asymmetric boundary conditions, i.e., in the vicinity of a free surface. This type of flow is relevant for many civil and marine engineering applications. For example, bridge decks during river flood or tsunami events may become partially or fully submerged (Malavasi and Guadagnini, 2003); Hydrokinetic turbines for river current applications operate near the water surface and their performance is affected by the surface (Liu et al., 2016). Two parameters of interests in this study are the width-to-length ratio,  $w/l$  (where  $w$  and  $l$  are the width and length of the rectangular cylinder, respectively), and the depth-to-length ratio,  $d/l$  (where  $d$  is the distance between the undisturbed surface and the top of the rectangular cylinder).

The unbounded flow past rectangular cylinders is classified by the

absence or presence of reattachment of the shear layers depending on  $w/l$ . As archived by a number of papers (Nakaguchi et al., 1968; Norberg, 1993; Sohankar, 2008), the value 2.8 marks the flow change from separated to reattached. With the change of the flow, the Strouhal number, which reflects the vortex shedding frequency, varies abruptly. Shimada and Ishihara (2002) reported two discontinuities in the Strouhal number at  $w/l = 2.8$  and  $w/l = 6.0$  through using a modified  $k-\epsilon$  model. They provided a division of the flow around rectangular cylinders: “separated” ( $w/l < 2.8$ ), “intermittently reattached” ( $2.8 < w/l < 6.0$ ) and “fully reattached” ( $w/l > 6.0$ ). Besides, Okajima (1982) argued that for rectangular cylinders with  $w/l$  equal to 2.0 and 3.0, there was found to be a certain range of  $Re$  where a discontinuity in the Strouhal number occurs. An explanation for this is the change of the flow from steadily reattached to occasionally reattached or separated as  $Re$  increases in the range from 70 to  $2.0 \times 10^4$ .

With the introduction of an asymmetric boundary condition, the flow around rectangular cylinders and consequently the force are affected, causing deviations from the infinite-medium reference case. Relevant to the present study is the flow past cylinders near a wall. Bosch et al. (1996) found based on experiments that when the gap-to-length ratio,  $G/l$ , decreases from 1.5 to 0.75, the flow from a square cylinder becomes

\* Corresponding author. College of Civil Engineering, Hunan University, Changsha, 410082, Hunan, China.

E-mail address: [denglu@hnu.edu.cn](mailto:denglu@hnu.edu.cn) (L. Deng).

<https://doi.org/10.1016/j.oceaneng.2020.107049>

Received 29 June 2019; Received in revised form 12 January 2020; Accepted 30 January 2020

Available online 18 February 2020

0029-8018/© 2020 Elsevier Ltd. All rights reserved.

Nomenclature	
$\alpha$	volume fraction
$C_{\alpha 1}, C_{\beta 1}, \beta^*, \sigma_{k1}, \sigma_{\omega 1}, C_{\alpha 2}, C_{\beta 2}, \sigma_{k2}, \sigma_{\omega 2}$	constants
$C_D$	drag coefficient
$C_L$	lift coefficient
$C_{Lrms}$	root-mean-square of the lift coefficient
$C_p$	pressure coefficient
$C_\mu$	constant
$d$	distance between the undisturbed surface and the top of the rectangular cylinder (m)
$d/l$	depth-to-length ratio
$f_\sigma$	pressure gradient due to surface tension (N/m <sup>3</sup> )
$Fr$	Froude number, $Fr = U/(gd)^{0.5}$
$F_1$	blending function $g$ acceleration due to gravity (m/s <sup>2</sup> )
$G$	gap between the wall and the bottom of the rectangular cylinder (m)
$G/l$	gap-to-length ratio
$I$	turbulence intensity
$k$	turbulent kinetic energy (m <sup>2</sup> /s <sup>2</sup> )
$\kappa$	mean curvature of the air-water interface (m <sup>-1</sup> )
$L$	turbulence length (m)
$p$	pressure (N/m <sup>2</sup> )
$p_{ref}$	reference pressure at the inlet boundary (N/m <sup>2</sup> )
$p_{rgh}$	modified pressure (N/m <sup>2</sup> )
$\rho$	density of the fluid (kg/m <sup>3</sup> )
$\tilde{P}_k$	production of the turbulent kinetic energy (N/(m <sup>2</sup> ·s))
$Re$	Reynolds number, $Re = Ul/\nu$
$\sigma$	surface tension coefficient (N/m)
$S_r$	magnitude of the strain rate (s <sup>-1</sup> )
$St$	Strouhal number, $St = fl/U$
$U$	inlet velocity of the water (m/s)
$u_c$	compression velocity (m/s)
$u_i, u_i'$	mean velocity and fluctuating component of the velocity in the $x_i$ direction (m/s)
$\mu$	dynamic viscosity of the fluid (N·s/m <sup>2</sup> )
$\nu$	kinematic viscosity of the fluid (m <sup>2</sup> /s)
$\nu_t$	turbulent eddy viscosity (m <sup>2</sup> /s)
$w, l$	width and length of the rectangular cylinder (m)
$w/l$	width-to-length ratio $\omega$ specific turbulence dissipation (s <sup>-1</sup> )
$y^+$	normalized distance to the wall

strongly affected by the wall, which is characterized by the asymmetric shedding motion. When  $G/l$  is lower than a critical value, the vortex shedding is suppressed. Bosch et al. (1996) reported that the critical  $G/l$  is in the range from 0.35 to 0.5 representing a transition rather than a sharp change. Martinuzzi et al. (2003) studied the influence of wall proximity on the flow past a square cylinder ( $Re = 2.2 \times 10^4$ ) and identified four flow regimes depending on  $G/l$ : (a) negligible influence from the wall ( $G/l > 0.9$ ); (b) increased wall influence ( $0.6 < G/l < 0.9$ ); (c) transition between regular vortex shedding and vortex suppression ( $0.3 < G/l < 0.6$ ); and (d) suppressed vortex shedding ( $G/l < 0.3$ ). Similar flow phenomena arise for circular cylinders approaching a wall. Price et al. (2002) classified four patterns of flow around a circular cylinder near a wall ( $1200 \leq Re \leq 4960$ ): (a) negligible influence on the vortex shedding and no separation of the wall boundary layer ( $G/l > 1.0$ ); (b) onset of the vortex shedding from the cylinder ( $0.5 < G/l < 0.75$ ); (c) pairing between the lower shear layer from the cylinder and the separated wall boundary layer ( $0.125 < G/l < 0.5$ ); and (d) suppressed vortex shedding ( $G/l < 0.125$ ). The difference between the limits of different flow regions reported by Martinuzzi et al. (2003) and Price et al. (2002) is mostly due to the different cross-sections. Wang and Tan (2008) demonstrated that the wake spreading and momentum exchange of square cylinders are lower than those of circular cylinders at the same  $G/l$  due to a more straightened effect of the shear layers in the former case. Angrilli et al. (1982) observed the asymmetric distribution of mean velocity across the wake when a circular cylinder locates near a wall. Lei et al. (2000) conducted a study of the suppressed vortex shedding past circular cylinders over a broad range of  $G/l$  for different  $Re$  ranging from 80 to 1000. They found that at low  $G/l$ , due to the contact of the lower shear layer from the cylinder and the separated wall boundary layer, the vorticity in the lower shear layer is cancelled by the opposite-signed vorticity in the wall boundary layer. Thus, the lower shear layer loses the strength to roll up and interact with the upper shear layer, and the vortex shedding is suppressed. Rashidi et al. (2016b) summarized nine categories of methods for controlling the wake destructive behavior and suppressing the vortex shedding behind bluff objects, including active methods, e.g., introducing external objects in one of the shear layers, imposing self-oscillation on the objects and utilizing electric, magnetic or thermal effects (Bovand et al., 2016; Rashidi et al., 2015, 2016a; Rashidi and Esfahani, 2015), and passive

methods, e.g., modifying surface roughness and approaching a plane boundary (Lei et al., 2000). Goktun (1975) found that on reducing  $G/l$ , the drag coefficient of circular cylinders first increases before rapidly decreases, and the peak drag coefficient occurs at around  $G/l = 0.5$ . The lift coefficient, on the other hand, increases monotonically with  $G/l$ . Goktun (1975) also observed an initial increase in the Strouhal number as  $G/l$  decreases to 0.5 and a drop at lower  $G/l$ , which reflects the occurrence of the suppressed vortex shedding.

Directly related to the present study is the flow past a cylinder near a free surface. Sheridan et al. (1997) studied the flow around a circular cylinder close to a free surface and observed that the surface jet develops at plenty of  $d/l$  and  $Fr$  combinations other than the pair reported in Sheridan et al. (1995). Sheridan et al. (1997) reported that the jet of fluid passing over the circular cylinder exhibits three metastable states: (a) attachment to the free surface; (b) attachment to the cylinder; and (c) an intermediate state in between. Each state was found to possess limited stability and switches to other state spontaneously with a low non-dimensional frequency of the order of  $10^{-3}$ . The same flow problem has been investigated by Reichl et al. (2005) who focused more on physical parameters such as shedding frequency, forces, etc. Reichl et al. (2005) found that the surface jet emerges owing to the local high  $Fr$  (approaching unity) which results from the combined effects of the locally increased velocity and the lowered water surface. They also pointed out that the suppression of vortex shedding accompanying the surface jet is because of the surface vorticity entering the wake and cross-annihilating the wake vorticity. Reichl et al. (2005) plotted a map showing the occurrence or non-occurrence of vortex shedding as functions of  $Fr$  and  $d/l$ . The surface jet has also been observed for a plate with  $w/l = 0.1$  in the vicinity of a free surface (Liu et al., 2016). Liu et al. (2016) found that as  $d/l$  decreases, the wake structures behind the plate become irregular and a jet-like flow forms from the surface on top of the plate when  $d/l$  is 0.3 ( $Re = 5.0 \times 10^4$ ). The suppressed vortex shedding was observed by Zhong et al. (2019) who studied the flow past rectangular cylinders with  $w/l$  equal to 1.0 and 3.0 close to a free surface ( $Re = 2.5 \times 10^4$ ) but the surface jet was not displayed in their study. Most papers on the flow past rectangular cylinders near a free surface focus more on the force aspects. Liu et al. (2016) reported that the drag coefficient of the plate ( $w/l = 0.1$ ) reduces as  $d/l$  decreases and a dramatic reduction occurs between  $d/l = 0.6$  and  $d/l = 0.5$ . Similar variations of

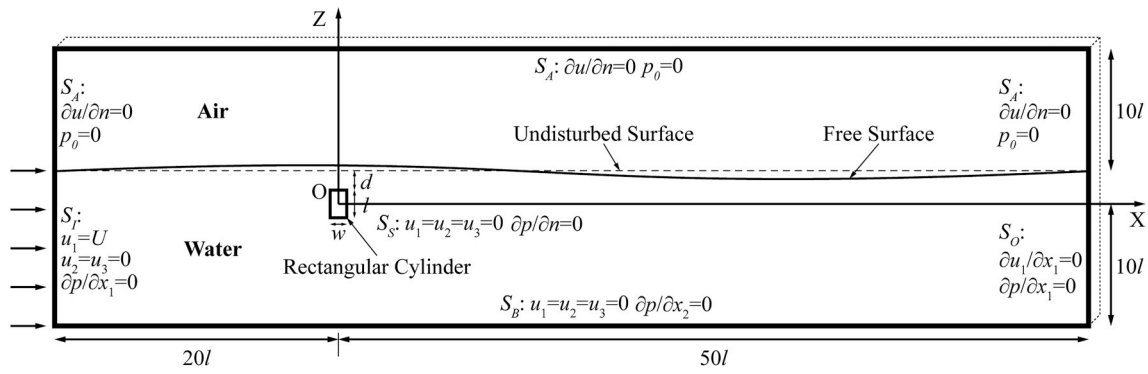


Fig. 1. The computational domain and the boundary conditions.

the drag coefficient with  $d/l$  were observed for circular cylinders near a free surface, except that the critical  $d/l$  at which the drag coefficient decreases sharply is about 0.4 (Miyata et al., 1990). Malavasi and Guadagnini (2007) experimentally investigated the interaction between the free surface and a submerged rectangular cylinder with  $w/l$  equal to 3.0. They reported that when the water depth is fixed at  $7.0l$ , the drag coefficient of the cylinder increases as  $d/l$  decreases from 4.5 to 0 while the lift coefficient approximately levels from  $d/l = 4.5$  to  $d/l = 1.5$  and decreases from  $d/l = 1.5$  to  $d/l = 0$ . Zhong et al. (2019) indicated that the disagreement between the variations of force coefficients with  $d/l$  reported by Liu et al. (2016) and Malavasi and Guadagnini (2007) is attributed to the difference in  $w/l$ . Zhong et al. (2019) concluded that there is a close connection between the effects of  $d/l$  and  $w/l$ . They also reported that the drag coefficient of the square cylinder first increases and then decreases sharply as  $d/l$  decreases, and the Strouhal number varies slightly for most  $d/l$  but drops suddenly when  $d/l$  decreases passing a critical value. The force variations of the square cylinder with  $d/l$  reported by Zhong et al. (2019) are very similar to those of circular cylinders approaching a wall reported by Goktun (1975). Although the flow structures and force coefficients of rectangular cylinders with some  $w/l$  near a free surface have been investigated, e.g., Liu et al. (2016), Malavasi and Guadagnini (2007) and Zhong et al. (2019), a comprehensive study of rectangular cylinders with various  $w/l$  approaching a free surface has not been conducted. Particularly, classifications of the flow depending on  $d/l$  and  $w/l$  have not been tackled. Besides, a clear demonstration of the relation between the flow behaviors and the force variations with  $d/l$  is also lacking.

In the present study, numerical simulations of flow past rectangular cylinders beneath the free surface are conducted using the computational fluid dynamics (CFD) method. The Reynolds-averaged Navier-Stokes (RANS) approach is adopted. The turbulence is modeled with the Mentor shear stress transport (SST)  $k - \omega$  model (Menter, 1994) and the free surface evolution is captured with the volume of fluid (VoF) multiphase model (Hirt and Nichols, 1981). A broad range of  $d/l$  (0.3–4.5) and  $w/l$  (0.7–5.0) is considered. The flow structures, velocity field and force coefficients are analyzed. Flow results show that the anti-symmetric vortex shedding becomes asymmetric when the

rectangular cylinder approaches a free surface. Three patterns of asymmetric flow depending on  $w/l$  are observed: “asymmetrically separated”, “one-sidedly reattached” and “asymmetrically reattached”. The vortex shedding is suppressed when  $d/l$  is lower than a critical value. The variations of force coefficients with  $d/l$  for rectangular cylinders with  $w/l$  in the ranges of  $0.7 < w/l < 1.5$ ,  $1.5 \leq w/l < 2.8$  and  $2.8 < w/l \leq 5.0$  show different trends due to the occurrence of different asymmetric flows associated with the three  $w/l$  ranges. The boundaries between different flow patterns are defined based on the variations of the force coefficients with  $d/l$ . The findings from the present study provide a deep understanding of the flow and forces of structural members with a rectangular cross-section located close to the free surface.

The remainder of the paper is organized as follows. The physics of the flow problem is described in the following section. Details of the numerical simulations are provided in section 3. The simulation results, including the flow results, velocity field and forces, and their discussions are presented in section 4. Finally, the concluding remarks are given in section 5.

## 2. Problem description

Two-dimensional simulations of flow past rectangular cylinders near the water surface are conducted. A schematic of the computational configuration and the coordinate system is drawn in Fig. 1. The coordinate system is fixed at the center of the rectangular cylinder with the  $x$  axis aligned with the inlet flow direction. The inlet and outlet are  $20l$  upstream and  $50l$  downstream of the cylinder, respectively. The entire domain is composed of air on the top and water at the bottom. The top boundary is  $10l$  away from undisturbed free surface and the bottom is  $10l$  away from the cylinder center. The rectangular cylinder is placed beneath the surface. The distance between the undisturbed surface and the top of the rectangular cylinder denoted by  $d$  has a significant impact on the flow and forces of the cylinder. Details of the sizes of the rectangular cylinder along with other parameters used in the simulations are presented in Table 1. Note that the  $Re$  value selected in the present simulations is  $2.5 \times 10^4$ , which would be in the order of  $10^7$  for a full-

Table 1

Details of the parameters used in the simulations.

Parameters	Symbol	Value
Length of the rectangular cylinder	$l$	0.10 m
Width of the rectangular cylinder	$w$	0.07 m–0.50 m
Width-to-length ratio	$w/l$	0.7–5.0
Distance between the undisturbed surface and the top of the rectangular cylinder	$d$	0.03 m–0.45 m
Depth-to-length ratio	$d/l$	0.3–4.5
Inlet velocity of the water	$U$	0.25 m/s
Kinematic viscosity of the water	$\nu$	$1.01 \times 10^{-6} \text{ m}^2/\text{s}$
Reynolds number	$Re$	$2.5 \times 10^4$
Density of the water	$\rho$	1000 $\text{kg}/\text{m}^3$

scale model, and thus is of significance to engineering applications.

The following assumptions are made in the present study. 1. The flow is two-dimensional, incompressible, viscous and turbulent. Two-dimensional simulations are employed due to the significance of two-dimensional flow structures when the rectangular cylinder with  $w/l > 0.7$  approaches a free surface (Zhong et al., 2019). 2. The distance between the rectangular cylinder and the outlet is assumed to be sufficiently large such that the outlet effects on the wake structures are negligible (Liu et al., 2016; Sohankar, 2008).

### 3. Numerical simulations

#### 3.1. Governing equations

The simulation of free surface flows involves modeling two immiscible fluids, i.e., water and air. In the present simulations, the VoF model (Hirt and Nichols, 1981) is adopted to capture the surface evolution. One notable advantage inherent in the model's surface capturing is static mesh allowance, which makes this method popular among CFD practitioners and engineers. Applicability of the VoF method (Hirt and Nichols, 1981) in modeling regular or irregular waves was demonstrated by Higuera et al. (2013a), Hu et al. (2016), Jacobsen et al. (2012) and Machado et al. (2018), and its engineering applications were explored by Bruinsma et al. (2018), Higuera et al. (2013b) and Martínez-Ferrer et al. (2018). The surface capturing in VoF (Hirt and Nichols, 1981) is realized through introducing the volume fraction, which varies from 0 to 1 according to the proportion of one fluid occupying the cell volume. A water cell is marked with  $\alpha = 1$ , an air cell is marked with  $\alpha = 0$ , and the air-water interface is presented where  $0 < \alpha < 1$ . The classic advection equation of the volume fraction is given as

$$\frac{\partial \alpha}{\partial t} + \frac{\partial u_j \alpha}{\partial x_j} = 0 \quad (1)$$

In order to maintain a sharp air-water interface and guarantee the bounded  $\alpha$  between 0 and 1, an artificial compression term is integrated into equation (1), leading to

$$\frac{\partial \alpha}{\partial t} + \frac{\partial u_j \alpha}{\partial x_j} + \frac{\partial u_{cj} \alpha (1 - \alpha)}{\partial x_j} = 0 \quad (2)$$

where  $u_c$  is the relative velocity between water and air, designated as the "compression velocity". For further reference see Rusche (2003) and Ubbink (1997). With the introduction of the volume fraction, the fluid properties at each cell are evaluated in the form  $\phi = \alpha \phi_{water} + (1 - \alpha) \phi_{air}$ . For example, the density and dynamic viscosity of the fluid are calculated as  $\rho = \alpha \rho_{water} + (1 - \alpha) \rho_{air}$  and  $\mu = \alpha \mu_{water} + (1 - \alpha) \mu_{air}$ , respectively.

The continuity and Navier-Stokes (N-S) equations are averaged over time to derive the Reynolds-averaged equations for the conservation of mass and momentum of the fluid.

$$\frac{\partial u_j}{\partial x_j} = 0 \quad (3)$$

$$\begin{aligned} \frac{\partial \rho u_i}{\partial t} + \frac{\partial \rho u_i u_j}{\partial x_j} - \frac{\partial}{\partial x_j} \left( \mu \frac{\partial u_i}{\partial x_j} \right) - \frac{\partial u_i}{\partial x_j} \cdot \frac{\partial \mu}{\partial x_j} = - \frac{\partial p_{rgh}}{\partial x_i} - g x_j \frac{\partial \rho}{\partial x_j} + \mu \frac{\partial^2 u_i}{\partial x_j^2} + \sigma \kappa \frac{\partial \alpha}{\partial x_i} \\ - \frac{\partial \rho u_i u_j}{\partial x_j} \end{aligned} \quad (4)$$

where  $u_i$  and  $u_i'$  ( $i = 1, 2, 3$ ) denote the mean velocity and fluctuating component of the velocity in the  $x_i$  direction, respectively. The modified pressure  $p_{rgh}$  defined as  $p_{rgh} = p - \rho g \cdot \mathbf{x}$  is used in equation (4) in order to simplify the definition of pressure condition for each phase, i.e., air and water, at wall boundaries. The surface tension at the air-water interface is accounted for by the fourth term on the right-hand side of equation (4), which is evaluated per unit volume using the continuum surface

force (CSF) model (Ubbink, 1997).

$$f_\sigma = \sigma \kappa \nabla \alpha \quad (5)$$

where  $\sigma$  is the surface tension coefficient;  $\kappa$  is the mean curvature of the interface determined from the following expression.

$$\kappa = - \nabla \cdot \frac{\nabla \alpha}{|\nabla \alpha|} \quad (6)$$

The time-averaging process gives rise to the unknown Reynolds stress terms in the momentum equations (see equation (4)), bringing the benefits of using statistical analyses to account for turbulence effects. Although the accuracy of RANS relies on the statistical models, its favorable performance in industrial applications is acknowledged by the CFD community. Successful applications of RANS to high Reynolds number flows around bluff objects can be found in plenty of literatures, e.g., Mannini et al. (2010), Ong et al. (2009), Stringer et al. (2014) and Tian et al. (2013). The Reynolds stress terms in equation (4) are approximated with the Boussinesq equation, which is an essential equation for eddy-viscosity models that transforms the calculation of the Reynolds stress to the computation of the turbulent eddy viscosity. The Mentor SST  $k - \omega$  model (Menter, 1994) is adopted to compute the turbulent eddy viscosity in the present simulations. The turbulent eddy viscosity is obtained by solving two additional energy equations, i.e., the transport equations of the turbulent kinetic energy  $k$  and the specific turbulence dissipation  $\omega$ .

$$\frac{\partial k}{\partial t} + u_j \frac{\partial k}{\partial x_j} = \frac{\partial}{\partial x_j} \left( \left( \nu + \frac{\nu_t}{\sigma_k} \right) \frac{\partial k}{\partial x_j} \right) + \frac{1}{\rho} \tilde{P}_k - \beta^* k \omega \quad (7)$$

$$\begin{aligned} \frac{\partial \omega}{\partial t} + u_j \frac{\partial \omega}{\partial x_j} = \frac{\partial}{\partial x_j} \left( \left( \nu + \frac{\nu_t}{\sigma_\omega} \right) \frac{\partial \omega}{\partial x_j} \right) + \tilde{C}_\alpha \frac{\omega}{k} \nu_t \left( \frac{\partial u_i}{\partial x_j} + \frac{\partial u_j}{\partial x_i} \right) \frac{\partial u_i}{\partial x_j} - \tilde{C}_\beta \omega^2 \\ + 2(1 - F_1) \sigma_{\omega 2} \frac{1}{\omega} \frac{\partial k}{\partial x_j} \frac{\partial \omega}{\partial x_j} \end{aligned} \quad (8)$$

$$\nu_t = \frac{0.31k}{\text{Max}[0.31\omega, \sqrt{2}S, F_2]} \quad (9)$$

where  $\tilde{P}_k$  is the production of the turbulent kinetic energy and  $S_j$  is the magnitude of the strain rate. The constants in equations (7) and (8) depend on the blending function  $F_1$  in the form  $\tilde{\phi} = F_1 \phi_1 + (1 - F_1) \phi_2$ , where  $\phi_1$  and  $\phi_2$  are the corresponding constants in the original  $k - \omega$  and  $k - \epsilon$  models respectively. The constants of the original models are assigned the following values:  $C_{\alpha 1} = 0.5532$ ,  $C_{\beta 1} = 0.075$ ,  $\beta^* = 0.09$ ,  $\sigma_{k1} = 2.00$ ,  $\sigma_{\omega 1} = 2.00$ ,  $C_{\alpha 2} = 0.4403$ ,  $C_{\beta 2} = 0.0828$ ,  $\sigma_{k2} = 1.00$  and  $\sigma_{\omega 2} = 1.186$ . The calculation of the turbulent eddy viscosity by equation (9) is favorable as it guarantees that Bradshaw's assumption is satisfied (Moukalled et al., 2015).

#### 3.2. Numerical methods

The continuity and Reynolds-averaged N-S equations, the transport equation of the volume fraction and the turbulence model equations are discretized using the finite volume method (FVM) performed in the open source package OpenFOAM. OpenFOAM is a bundle of C++ libraries, designed to solve problems like fluid flows, combustion, electromagnetics, chemical reactions, etc. A comprehensive comparison between OpenFOAM and Ansys CFX-13.0 was given in Stringer et al. (2014). As stated in Moukalled et al. (2015), the FVM is implemented by integrating each term in the equations over a control volume and relating the volume integrals to the surface integrals using Gauss's theorem. The surface and volume integrals are both evaluated with the mid-point integration approximation which yields second order accuracy. The convective and diffusive fluxes at cell faces are evaluated with the second order upwind (SOU) and central differencing (CD) schemes, respectively. The second-order Crank-Nicolson (CN) scheme is used for

the time integration.

The interFoam solver in OpenFOAM is adopted. The interFoam is capable of solving two-phase flow problems using the FVM discretization and the VoF method (Hirt and Nichols, 1981). A detailed flow chart describing this solver was given in Higuera et al. (2013a). The interFoam employs the PIMPLE algorithm to treat the pressure-velocity coupling problem. The principal of the algorithm is as follows (Holzmann, 2016): within each time step, both the inner pressure correction loop (PISO loop) and outer pressure-momentum correction loop (SIMPLE loop) are executed. In the inner loop, the pressure is recalculated with the new updated flux. In the outer loop, the velocity matrix is first rebuilt with the new flux, the pressure is then corrected with the new velocity matrix and the flux is finally corrected with the new pressure. The calculations are repeated until convergence is achieved. A visual description of the PIMPLE algorithm is referred to Higuera et al. (2013a). In the present simulations, three inner loops and three outer loops are executed within each time step. The solutions are regarded as being converged when the residuals of the velocity and pressure are lower than 1e-06.

### 3.3. Boundary and initial conditions

The fluid domain boundaries include the inlet  $S_I$ , the outlet  $S_O$ , the atmosphere  $S_A$ , the bottom  $S_B$  and the structural surface  $S_S$  as shown in Fig. 1. At the inlet, a uniform velocity  $u_1 = U$  is imposed and the pressure is set to zero normal gradient. The volume fraction at the water inlet is set to 1, and  $k$  and  $\omega$  are given by

$$k = 1.5(UI)^2 \quad (10)$$

$$\omega = k^{0.5} / (C_\mu^{0.25} L) \quad (11)$$

where  $I$  ( $= 5\%$ ) is the turbulence intensity and  $L$  ( $= 0.07l$ ) is the turbulence length. The empirical constant  $C_\mu$  is 0.09.

At the outlet, zero normal gradient conditions are applied to all variables. At the atmosphere, a constant total pressure is prescribed. The pressure adjusts according to the velocity as  $p_0 = p + 0.5\rho|u|^2$ . At the surface of the rectangular cylinder and at the bottom, no-flux and no-slip boundary conditions are specified for the velocity, and the pressure is set to be zero gradient. In order to reduce the computing time, wall functions are used in the near-wall region. The first internal grid point is placed in the inertial layer ( $11.06 < y^+ < 200.00$ ) where the empirical relations apply (Moukalled et al., 2015).

The initial velocities in the air and water portion of the computational domain are set to zero and the inlet velocity  $U$ , respectively.

### 3.4. Convergence study

The meshes are generated by an algebraic method. Fig. 2 shows that the grid is fully orthogonal and dense areas of the grid points appear in the region near the rectangular cylinder and the free surface. A small mesh size near the rectangular cylinder is chosen ( $\delta x = 1/40l$ ). This small mesh size is used in the region between  $0.5l$  upstream and  $3.0l$  downstream of the cylinder (see Fig. 2(b)), and increases toward the inlet or outlet with a low ratio (see Fig. 2(a)). A grid convergence study is conducted for four cases ( $d/l = 0.3$  and  $w/l = 1.0$ ;  $d/l = 0.3$  and  $w/l = 5.0$ ;  $d/l = 4.5$  and  $w/l = 1.0$ ;  $d/l = 4.5$  and  $w/l = 5.0$ ). Details of the convergence study are referred to Zhong et al. (2019). The medium

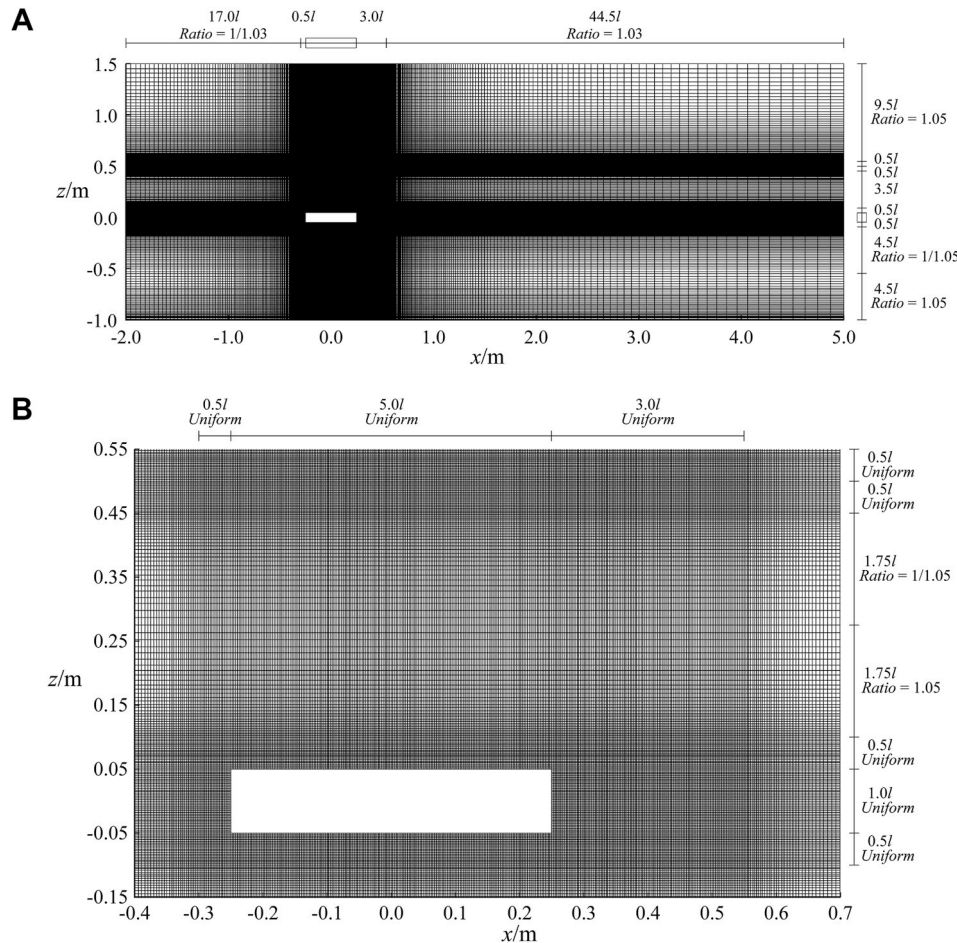


Fig. 2. The mesh generation for the case of  $d/l = 4.5$  and  $w/l = 5.0$ : (a) Overall view; (b) Local view.

mesh densities are chosen for all the cases in the present simulations considering the tradeoff between accuracy and computing time. In the present study, the time-averaged drag and lift coefficients are calculated over the time period 300s–400s and 200s–300s when  $d/l$  is lower and higher than 1.0, respectively (Zhong et al., 2019). In addition, the distance of the first internal grid point to the wall is selected to be  $0.025 l$  at the surface of the rectangular cylinder and  $0.050 l$  at the bottom, respectively. The time-averaged  $y^+$  around the surface of the cylinder is between 11.06 and 50.00, indicating that the first internal grid points are located in the logarithmic layer.

## 4. Results and discussion

### 4.1. Validation of the numerical procedure (Anti-symmetric vortex shedding)

The numerical procedure is validated by comparing the present results with the published results. The cases with  $d/l = 4.5$  are used for the validation. With  $d/l$  equal to 4.5, the influence of the free surface on the flow around rectangular cylinders is considered weak (Malavasi and Guadagnini, 2007). The validation details are referred to Zhong et al. (2019). The validation test indicates that the present RANS simulations are capable of accurately predicting the force coefficients of rectangular cylinders when  $w/l \geq 0.7$ . Flow visualizations in Zhong et al. (2019) confirmed the capability of the two-dimensional simulations in reproducing the flow structures. A better visual representation of the flow is

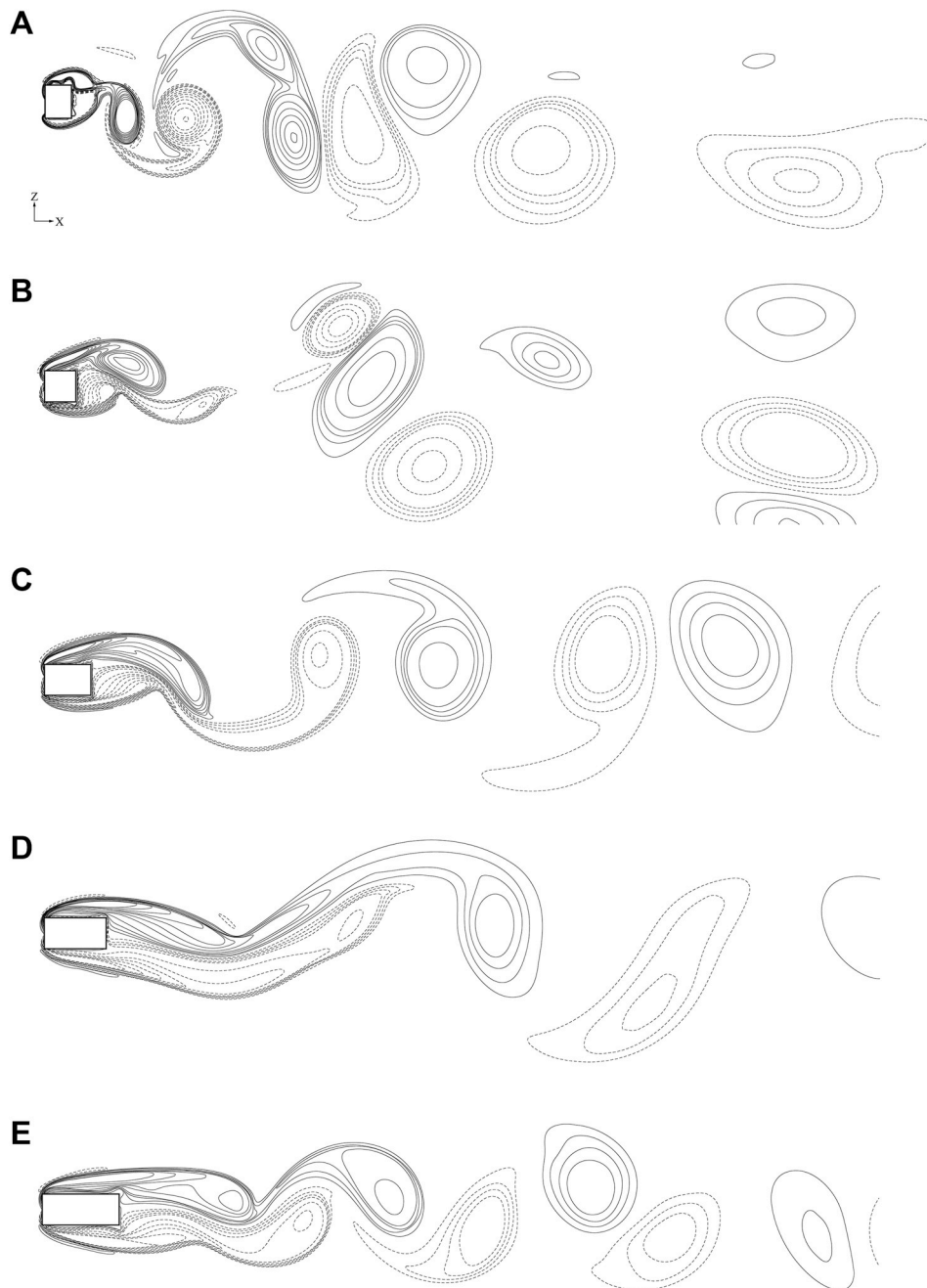


**Fig. 3.** Instantaneous vorticity contours around rectangular cylinders with various  $w/l$  located at  $d/l = 4.5$  when the lift is minimum: (a)  $w/l = 0.8$ ; (b)  $w/l = 1.0$ ; (c)  $w/l = 1.5$ ; (d)  $w/l = 2.0$ ; (e)  $w/l = 2.5$ ; (f)  $w/l = 3.0$ ; (g)  $w/l = 3.5$ ; (h)  $w/l = 4.0$ ; (i)  $w/l = 4.5$ ; (j)  $w/l = 5.0$ .

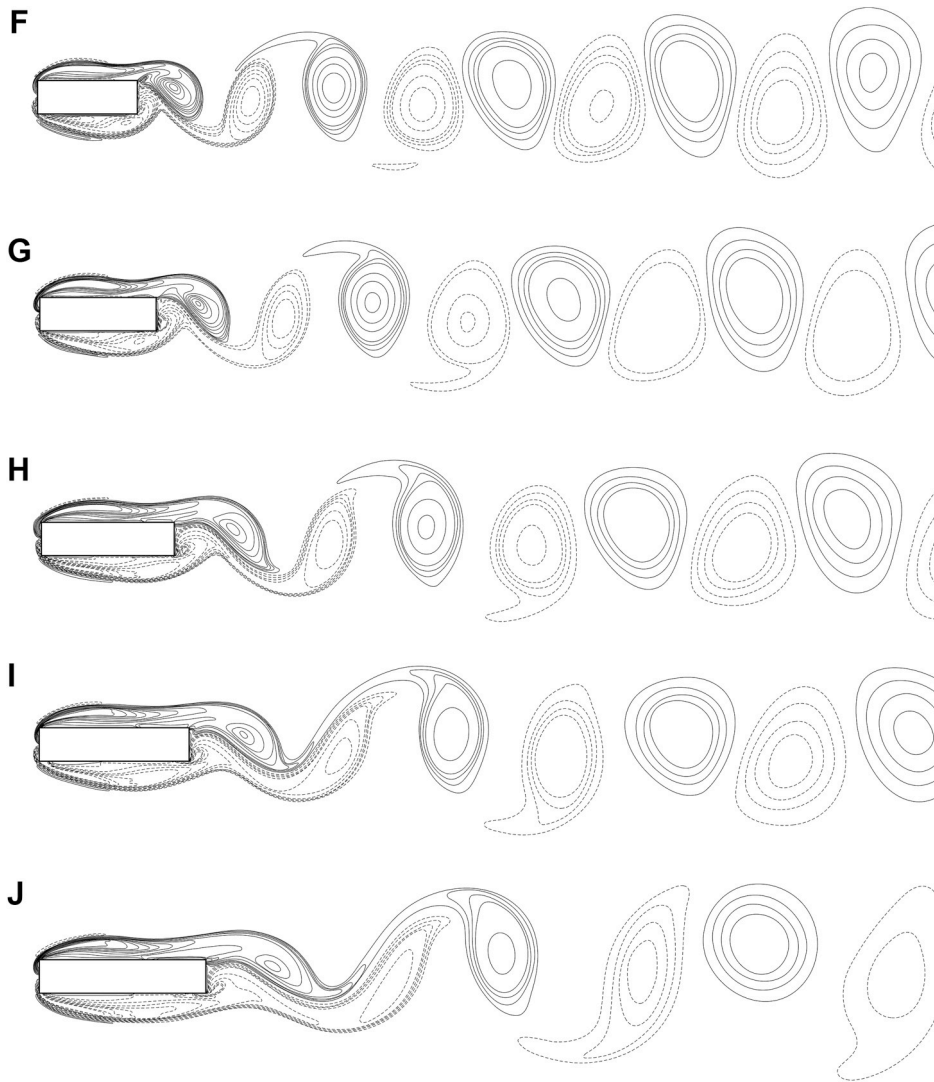


Fig. 3. (continued).

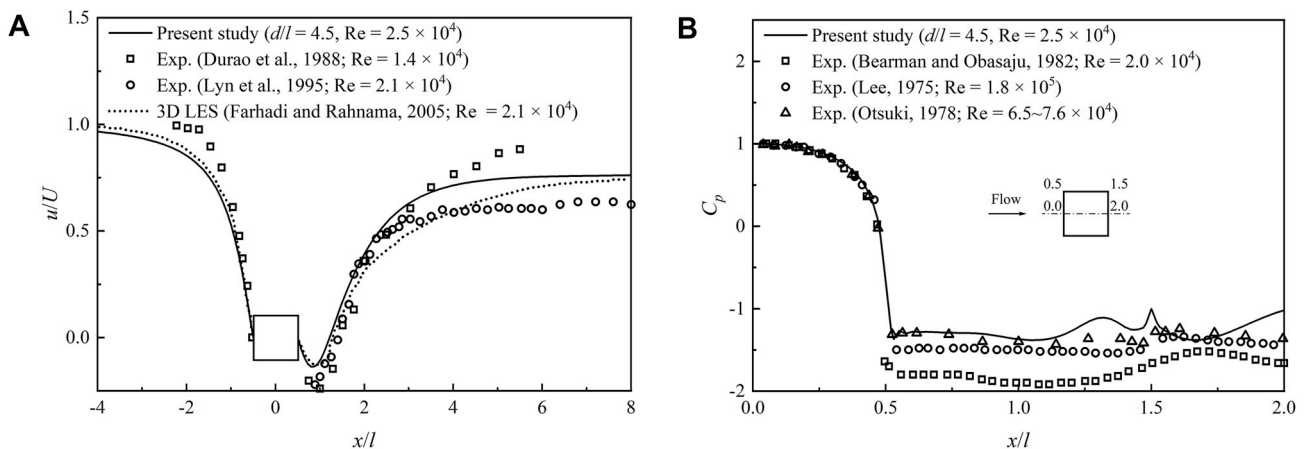


Fig. 4. Validation results: (a) Time-averaged streamwise velocity along the centerline of the rectangular cylinder with  $w/l = 1.0$  located at  $d/l = 4.5$ ; (b) Time-averaged pressure coefficient over the surface of the rectangular cylinder with  $w/l = 1.0$  located at  $d/l = 4.5$ .

illustrated in Fig. 3. The figures in Fig. 3 correspond to the instants when the lift is minimum. The solid and dashed contour lines represent the positive and negative vorticity contours, respectively. The agreement between the predicted flow and the flow results by Shimada and Ishihara

(2002) who used a modified two-dimensional  $k - \epsilon$  model and Sohankar (2006) who focused on the large eddy simulation (LES) is good. Particularly, the separated flow at  $w/l < 2.8$  and the reattached flow at  $w/l > 2.8$  are well reproduced by the present simulations.

Moreover, the velocity and pressure around the rectangular cylinder with  $w/l = 1.0$  are compared with the published results (Bearman and Obasaju, 1982; Durao et al., 1988; Farhadi and Rahnama, 2005; Lee, 1975; Lyn et al., 1995; Ohtsuki, 1978). Fig. 4(a) and (b) show the time-averaged streamwise velocity along the centerline of the square and the pressure coefficient over the surface of the cross-section, respectively. The pressure coefficient  $C_p$  is defined as

$$C_p = \frac{p - p_{ref}}{0.5\rho U^2} \quad (12)$$

where the reference pressure  $p_{ref}$  is taken as the pressure at the inlet boundary with the same depth as the square center.

Fig. 4(a) shows that the velocity upstream of the square and in the recirculation region is in agreement with the numerical results obtained by 3D LES (Farhadi and Rahnama, 2005). The velocity downstream of the square in near wake ( $1.0 \leq x/l \leq 3.0$ ) agrees with the experimental results by Durao et al. (1988) and Lyn et al. (1995), but in the intermediate wake ( $3.0 < x/l \leq 8.0$ ), there are differences between the present results and the experimental results (Durao et al., 1988; Lyn et al., 1995). The discrepancy is probably due to the different settings, e.g., Reynolds number and blockage ratio, in these studies. Simulation results in Fig. 4(b) indicate that the predicted pressure coefficient on the front side of the square ( $0.0 \leq x/l \leq 0.5$ ) agrees well with the experimental data (Bearman and Obasaju, 1982; Lee, 1975; Ohtsuki, 1978). The pressure coefficient on the upper and back sides ( $0.5 \leq x/l \leq 1.5$ ;  $1.5 \leq x/l \leq 2.0$ ) agrees with the results by Ohtsuki (1978), but is overpredicted comparing to the results by Bearman and Obasaju (1982) and Lee (1975). Overall, it is reasonable to believe that the present  $k - \omega$  model can give satisfactory predictions of the velocity and pressure for the square case.

It is worth mentioning that the vortex shedding around rectangular cylinders with  $w/l$  between 0.7 and 5.0 is anti-symmetric when the cylinder is located at  $d/l = 4.5$ . Fig. 3 shows that positive vortices with relatively higher strengths are shed from the upper corner of the leading edge when the lift is minimum. It will be shown that when the lift reaches maximum value, negative vortices with approximately equal strengths are formed at the lower corner of the leading edge. The symmetry of the flow is evidently demonstrated by the time-averaged vorticity contours as shown in Fig. 5. The occurrence of the anti-symmetric vortex shedding implies that when the rectangular cylinder is deeply submerged, e.g.,  $d/l = 4.5$ , the interaction between the free surface and the cylinder is weak. The weak interaction is also reflected

by the undisturbed water surface above the rectangular cylinder (not shown in Fig. 3).

## 4.2. Asymmetric vortex shedding

It has been documented that the unbounded flow past rectangular cylinders with  $w/l < 2.8$  and  $2.8 < w/l < 5.0$  is “separated” and “intermittently reattached”, respectively (Shimada and Ishihara, 2002). The separated flow is characterized by the periodic vortex shedding while the prominent feature of the reattached flow is the periodic reattachment of the vortices on the side surfaces. Besides, as reported by Okajima (1982), when  $w/l$  is between 2.0 and 2.8, a bimodal vortex shedding emerges accompanying the occasional reattachment of the separated shear layers onto the rearmost surfaces of the cross-sections. The difference between the flow past rectangular cylinders with different  $w/l$  causes significant differences in the interaction between the free surface and the cylinder. Observations on the present flow results reveal that with the approaching of a free surface, the anti-symmetric vortex shedding around the rectangular cylinder is affected and the flow becomes asymmetric. As  $w/l$  varies from 0.7 to 5.0, the asymmetric flow falls into three patterns, i.e., “asymmetrically separated”, “one-sidedly reattached” and “asymmetrically reattached”. Details on the three asymmetric flow patterns are discussed in the following.

### 4.2.1. Asymmetrically separated vortex shedding

Fig. 6 shows eight instants of vorticity around the rectangular cylinder with  $w/l = 1.0$  located at  $d/l = 0.7$ . The instants cover one cycle of vortex shedding and the time intervals between the instants are equal. The black line above the square denotes the free surface. It is seen in Fig. 6 that the separated flow around the square is asymmetric due to the effect of the free surface. Specifically, the constraint by the free surface above causes the overall downward movement of the vortices through pressing and pushing the upper and lower shear layers respectively. The positive vortices above the square are pressed and shed nearly in parallel with the surface. The negative vortices under the square are pushed downward and stretch in a direction away from the square. However, although the vortex shedding is asymmetric, the flow remains separated. The positive or negative vortices shed from the leading edge move across the square without reattaching the side surfaces. Moreover, the range of motion of the vortices about the square is narrowed and the centers of

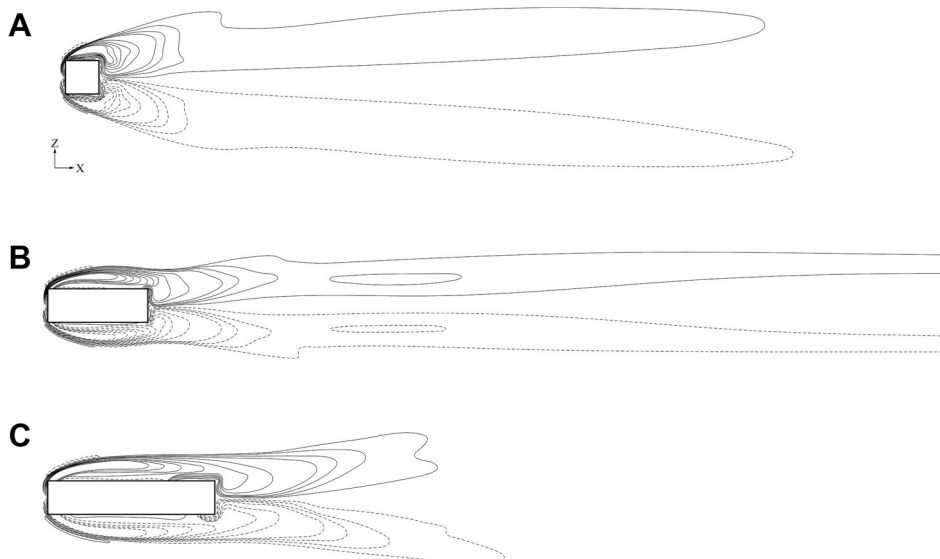
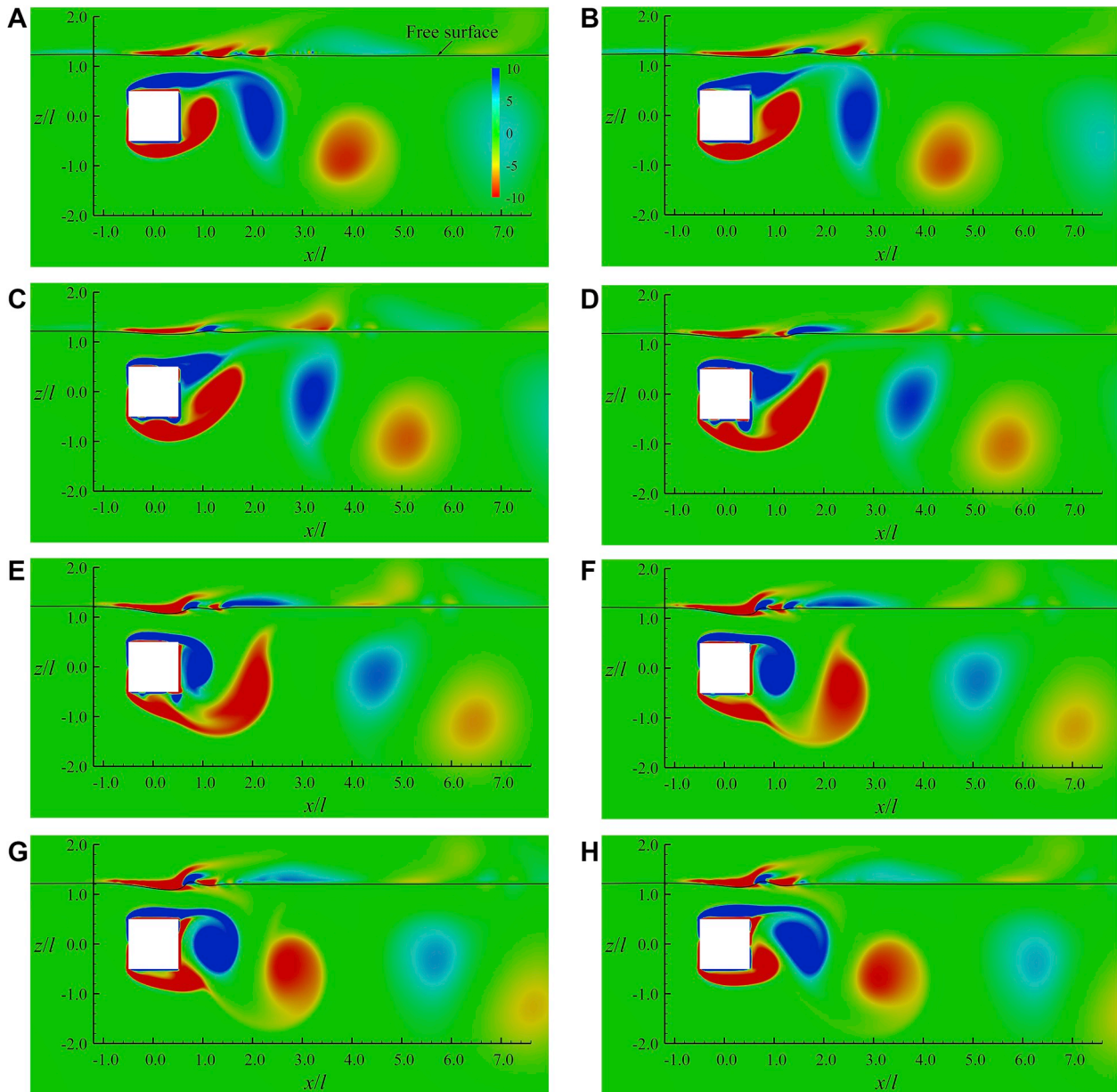


Fig. 5. Time-averaged vorticity contours around rectangular cylinders with  $w/l$  equal to (a) 1.0, (b) 3.0 and (c) 5.0 located at  $d/l = 4.5$ .



**Fig. 6.** Instantaneous vorticity around the rectangular cylinder with  $w/l = 1.0$  located at  $d/l = 0.7$ : (a) Instant 1 (at the minimum lift); (b) instant 2; (c) Instant 3; (d) Instant 4; (e) Instant 5 (at the maximum lift); (f) Instant 6; (g) Instant 7; (h) Instant 8.

both the positive and negative vortices lie closer to the trailing edge in comparison to the case when the square is deeply submerged. As a result, spacings between successively shed positive or negative vortices are reduced, indicating that the shedding frequency is enhanced. The asymmetrically separated flow, resulting from the unbalanced effects of the free surface on the shear layers above and under the square, represents a typical pattern of vortex shedding past rectangular cylinders with low  $w/l$  ratios near a water surface.

The time-dependent evolution of the free surface on top of the square is also depicted in Fig. 6. As shown in Fig. 6(a)–(e), when the lift varies from the minimum to the maximum, the free surface experiences an overall decline and a trough forms when the lift is maximum. The trough arises from the sinking of the water surface near the trailing edge, which is caused by the regression of the positive vortices above the square. The trough holds for a while and vanishes when the lift lowers back to minimum value. Fig. 6(e)–(h) show that as the lift varies from the maximum to the minimum, the free surface rises with the trough fading away gradually. The elevated surface results from the progression of the

positive vortices above the square.

#### 4.2.2. One-sidedly reattached vortex shedding

The asymmetric flow past rectangular cylinders with  $w/l$  between 1.5 and 2.8 shows different features from those when  $w/l$  is lower than 1.5 due to the occurrence of the one-sided flow reattachment. Fig. 7 illustrates this flow pattern through eight instants of vorticity during one cycle of vortex shedding past the rectangular cylinder with  $w/l = 2.5$  located at  $d/l = 1.0$ . As shown in Fig. 7, the positive vortices separated from the upper corner of the leading edge are pressed to reattach the rear portion of the upper surface, and by contrast, the negative vortices shed at the lower corner of the leading edge move away from the lower surface. The overall downward movement of the vortices is induced by the free-surface effect in a similar way to that of the asymmetrically separated flow, but the upper shear layer is reattached herein due to the relatively larger width of the rectangular cylinder. Note that the occasionally reattached shear layer above the rectangular cylinder with  $2.0 < w/l < 2.8$  reported in Okajima (1982) becomes constantly reattached

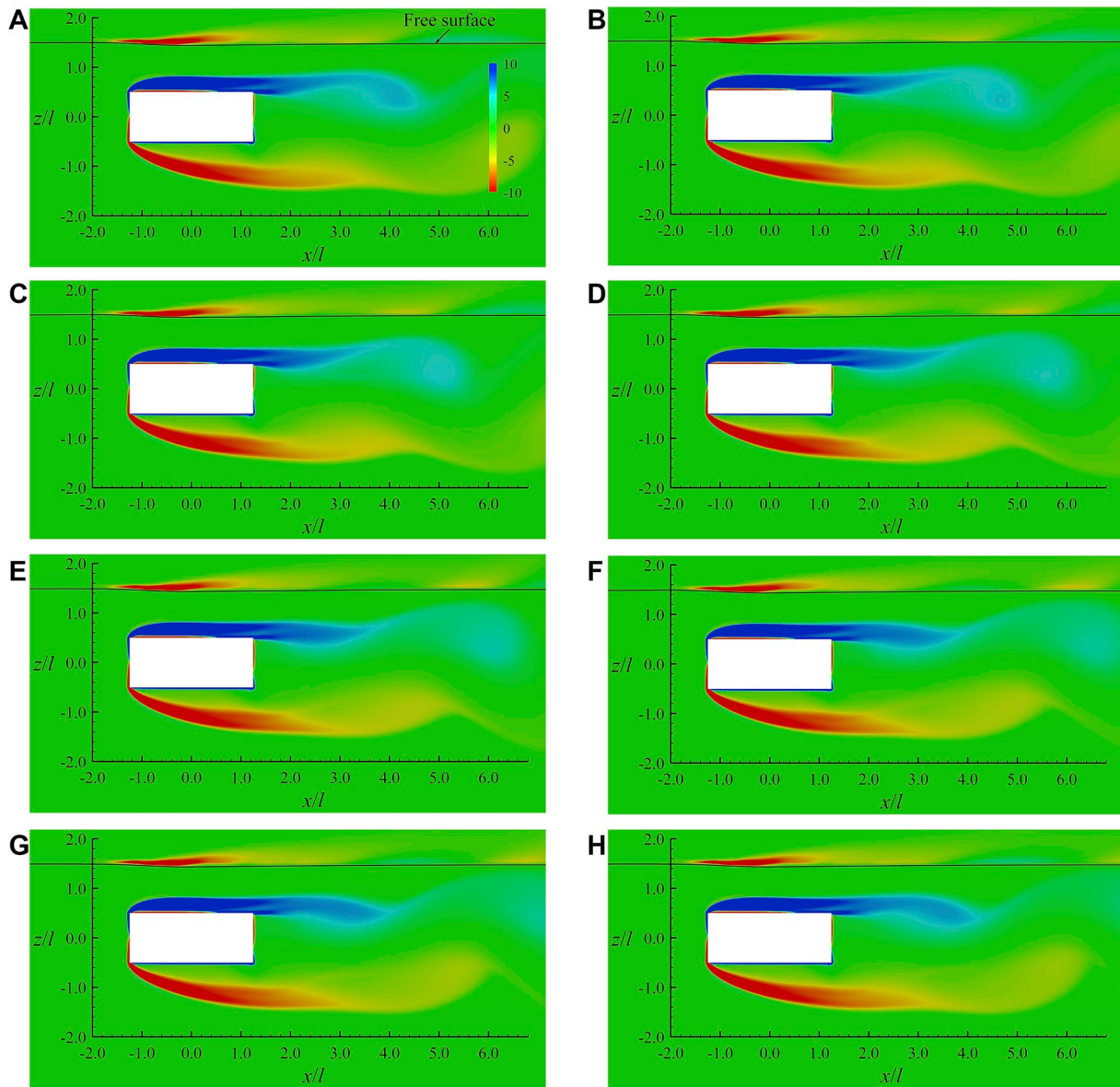


**Fig. 7.** Instantaneous vorticity around the rectangular cylinder with  $w/l = 2.5$  located at  $d/l = 1.0$ : (a) Instant 1 (at the minimum lift); (b) instant 2; (c) Instant 3; (d) Instant 4; (e) Instant 5 (at the maximum lift); (f) Instant 6; (g) Instant 7; (h) Instant 8.

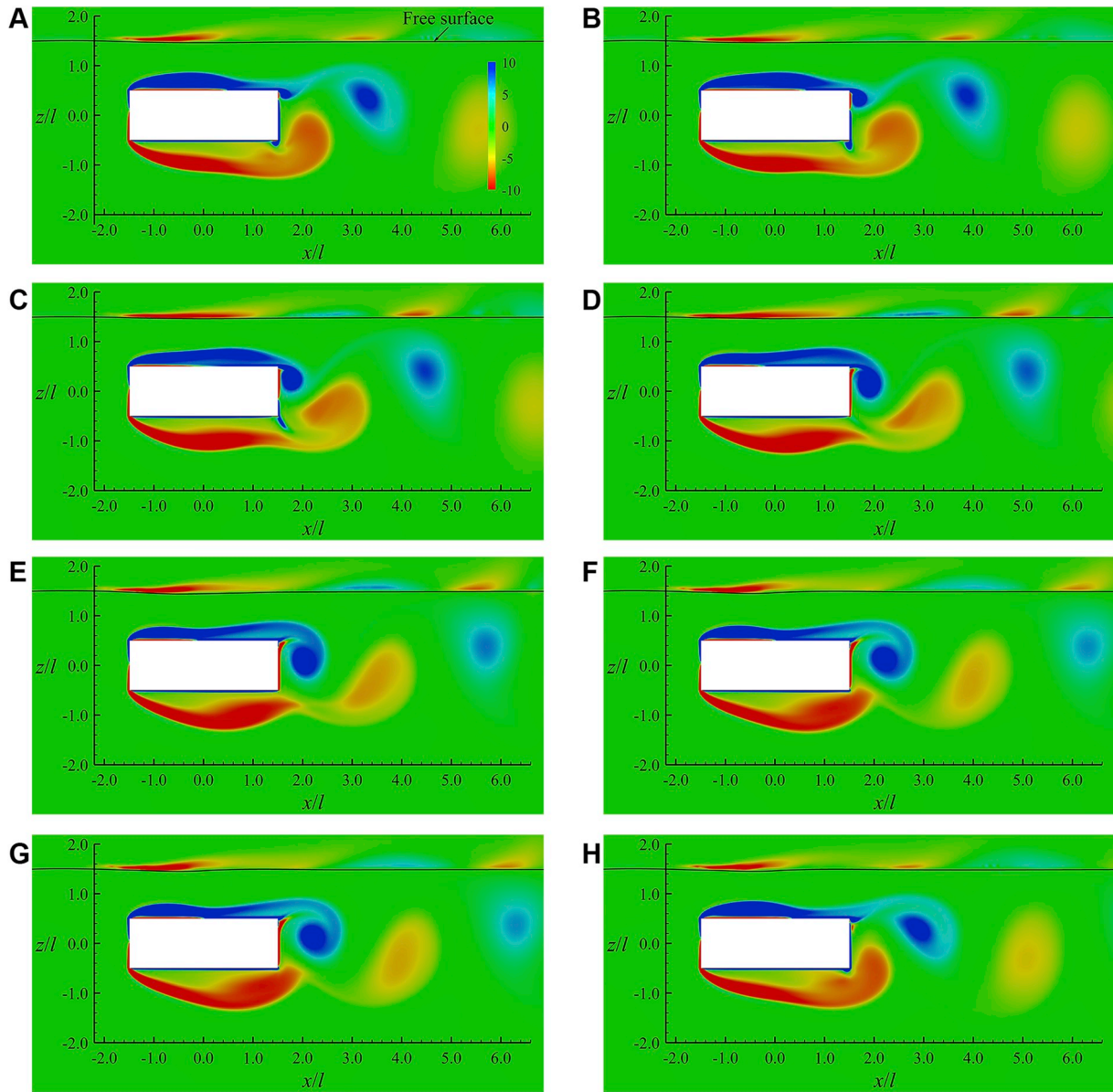
with the help of the free surface. The vortices around the rectangular cylinder are greatly lengthened due to the reattachment of the upper shear layer. The one-sided flow reattachment causes asymmetric vortical structures about the centerline of the cross-section in the wake. Fig. 7 indicates that the positive vortices produced at the upper corner of the trailing edge interact and join with the positive vortices shed from the leading edge, forming the wake structures that are different from those originated from the negative vortices shed along the lower surface. Despite the asymmetric vortex shedding, the vortices in the wake move almost in parallel with the free surface. Moreover, the vortex shedding frequency is enhanced as a result of the flow reattachment.

Fig. 7 also shows that fluctuations of the free surface are small and vary slightly over one cycle of vortex shedding, which is different from that in the asymmetrically separated flow (see Fig. 6). Fig. 7 demonstrates that due to the lengthened vortices, the regression and progression of the positive vortices above the rectangular cylinder are not as significant as the case with  $w/l = 1.0$ , in which the flow is asymmetrically separated. The water surface seems to be constrained by the rectangular cylinder and evolves slightly as the upper positive vortices shed

through. However, although the evolution of the surface is reduced, the significant free-surface effect on the vortex shedding is evident.

#### 4.2.3. Asymmetrically reattached vortex shedding

It was known that the flow past rectangular cylinders with  $w/l$  between 2.8 and 5.0 in an infinite domain is “intermittently reattached” (Shimada and Ishihara, 2002). As the rectangular cylinder approaches a free surface, the reattached flow becomes asymmetric. Fig. 8 shows eight instants of vorticity about the rectangular cylinder with  $w/l = 3.0$  located at  $d/l = 1.0$ . As shown in Fig. 8, the positive vortices shed from the upper corner of the leading edge are pressed, and as a result, the reattaching point of the vortices on the upper surface moves upstream. In contrast, the negative vortices produced at the lower corner of the leading edge are stretched downward with the reattaching point on the lower surface moving downstream. The pushing effect by the free surface above results in the asymmetry of the reattaching behaviors between the upper and lower shear layers. It is seen that the angle of the shedding direction of the positive vortices with respect to the upper surface when the lift is minimum (see Fig. 8(a)) is visibly smaller than



**Fig. 8.** Instantaneous vorticity around the rectangular cylinder with  $w/l = 3.0$  located at  $d/l = 1.0$ : (a) Instant 1 (at the minimum lift); (b) instant 2; (c) Instant 3; (d) Instant 4; (e) Instant 5 (at the maximum lift); (f) Instant 6; (g) Instant 7; (h) Instant 8.

that between the shedding direction of the negative vortices and the lower surface when the lift is maximum (see Fig. 8(e)). The asymmetric reattachment of the shear layers has little impact on the wake structures. As shown in Fig. 8, the positive and negative vortices in the wake move nearly in parallel with the free surface and are roughly symmetric. The vortex shedding frequency remains almost unvaried despite the asymmetric reattachment of the flow. Fig. 8 also shows similar surface fluctuations to those in the one-sidedly reattached flow (see Fig. 7).

#### 4.3. Suppressed vortex shedding

Reichl et al. (2005) reported that a jet-like flow forms around circular cylinders when the cylinder is placed in close proximity to a free surface. With the formation of the surface jet, the vortex shedding around the circular cylinder is suppressed. The suppression of vortex shedding is also observed in the flow around rectangular cylinders with various  $w/l$  when  $d/l$  is low. Fig. 9 shows the instantaneous vorticity about rectangular cylinders with  $w/l$  equal to 1.0, 2.5 and 3.0 located at  $d/l = 0.3$ . The flow is apparently different from that when the cylinder is

moderately or deeply submerged. As shown in Fig. 9, the positive vortices shed along the upper surface are significantly pressed and the negative vortices produced at the lower corner of the leading edge are forced to stretch away from the lower surface. The vortex shedding is suppressed while both the positive and negative vortices are greatly lengthened. The suppressed vortex shedding around a shallowly submerged rectangular cylinder has also been observed by Zhong et al. (2019) who reported that when  $d/l$  is lower than a critical value, the vortex shedding is suppressed due to the dominant free-surface effect. Reichl et al. (2005) plotted a map showing the occurrence or non-occurrence of vortex shedding as functions of  $Fr$  and  $d/l$ . In the present study, the existence or non-existence of vortex shedding past rectangular cylinders as functions of  $d/l$  and  $w/l$  is discussed and is used as a mean to distinguish the different flow patterns.

The time-dependent surface evolution on top of rectangular cylinders located at  $d/l = 0.3$  is different from that of the aforementioned flow patterns. As shown in Fig. 9, the water surface fluctuates significantly and the shape of the fluctuations resembles regular waves. The wave surface, beginning with a trough above the cylinder, spreads

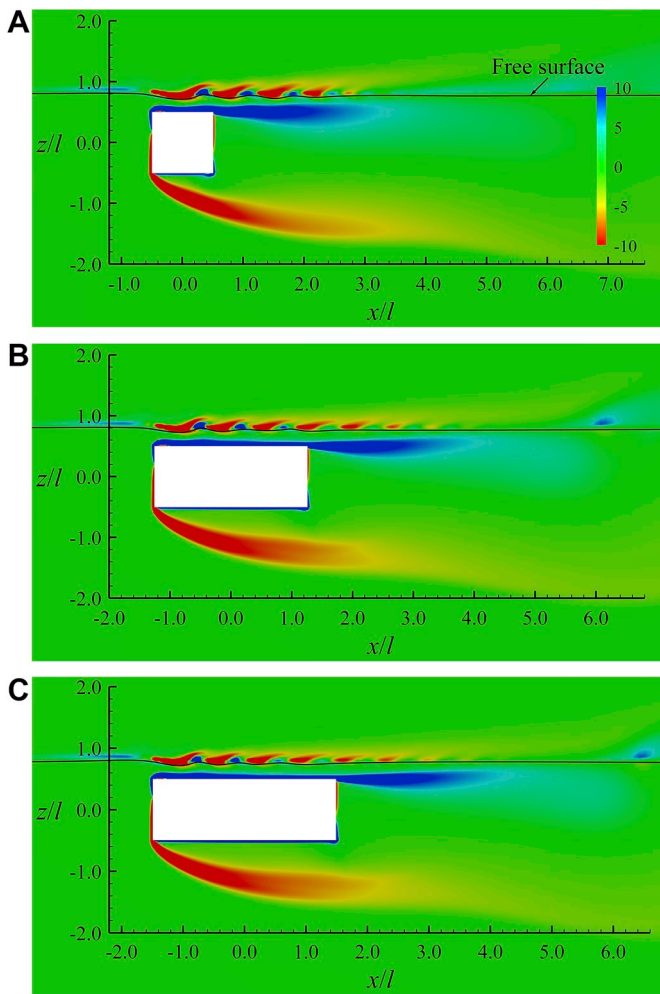


Fig. 9. Instantaneous vorticity around rectangular cylinders with  $w/l$  equal to (a) 1.0, (b) 2.5 and (c) 3.0 located at  $d/l = 0.3$  when the lift is minimum.

downstream and vanishes after several wave lengths. The shape of the surface varies slightly throughout. Fig. 9 also shows that significant vortices are generated at the free surface, which is similar to the jet-like flow past circular cylinders. However, in contrast to the dramatically curving surface in the jet-like flow which helps facilitate the transportation of surface vortices into the wake (Reichl et al., 2005), the surface fluctuations above rectangular cylinders are relatively small. The surface jet is not developed and the jet-like flow around rectangular cylinders is not observed. Thus, the vortices formed at the free surface are restricted by diffusion from moving a long distance and joining the wake while no extra contributions to facilitate the vertical movement of the vortices are received from the slightly curving surface. The interaction between the free surface and the rectangular cylinder is in the form of one-sided constraint from the surface and the vortex interaction between them is insignificant. Nevertheless, as revealed by an ongoing research by the present authors, when the Reynolds number is larger than a critical value, the surface curvature increases dramatically, leading to the development of surface jet. The formation of jet-like flow around rectangular cylinders has been observed by Liu et al. (2016) who investigated the flow past a plate with  $w/l = 0.1$ . The Reynolds number adopted by Liu et al. (2016) is  $5.0 \times 10^4$  which is higher than  $2.5 \times 10^4$  in the present study.

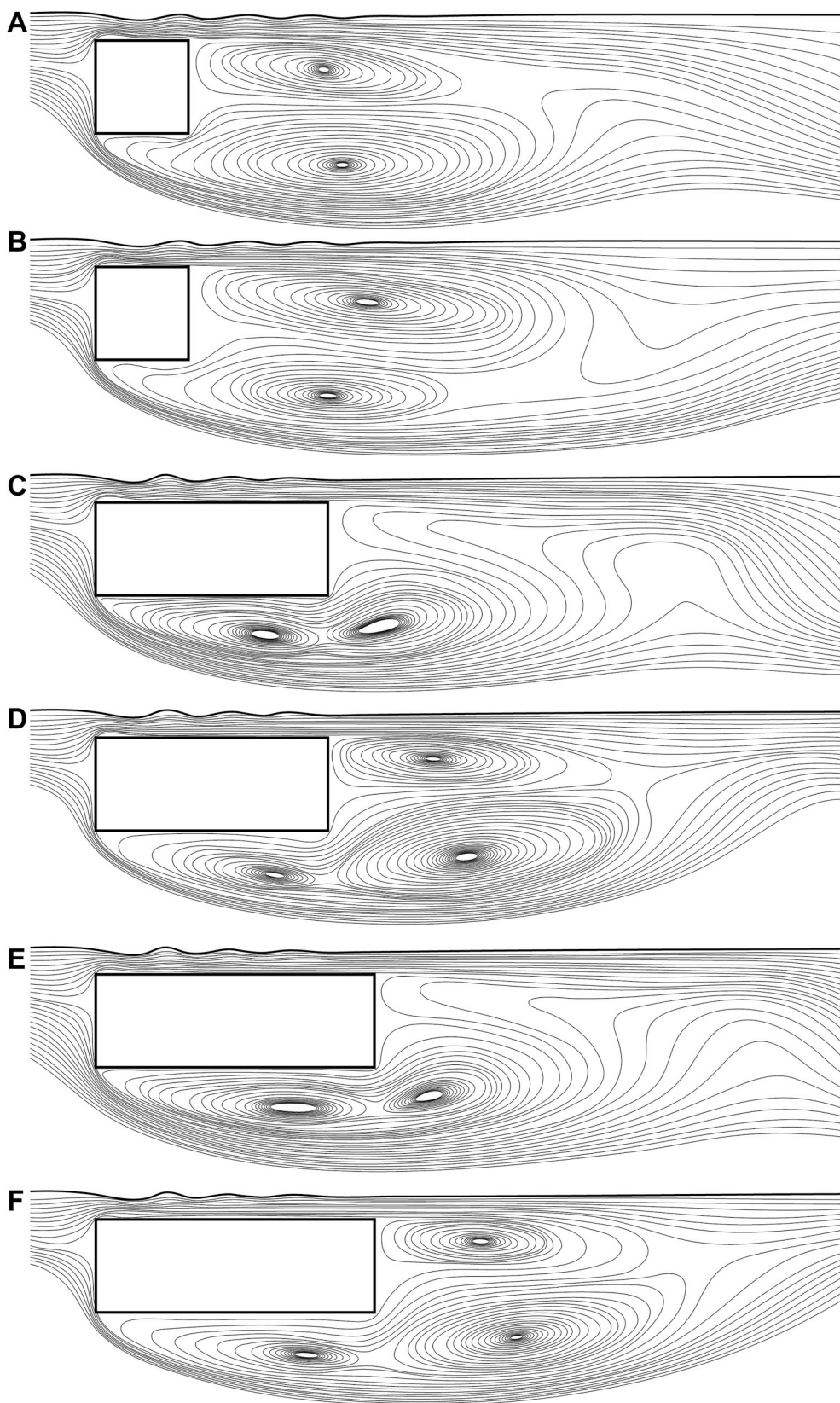
Lei et al. (2000) found that for a circular cylinder placed near a wall, the cessation of vortex shedding is due to the cancellation of the vorticity in the lower shear layer by the opposite-signed vorticity in the wall boundary layer, which prevents the lower shear layer from rolling up

and interacting with the upper shear layer. For a rectangular cylinder close to a free surface in the present research, the reduction of the vorticity in the upper shear layer is evident as shown in Fig. 9. Besides, it is important to note that the suppressed vortex shedding around rectangular cylinders is different from that around circular cylinders. The curved surface of circular cylinders permits the move of the point where the positive and negative vortices meet in the wake, and the flow is evidently skewed when the cylinder approaches a free surface. Thus, metastable behaviors display as the jet of fluid passes over the circular cylinder (Reichl et al., 2005). However, for rectangular cylinders, the flow is separated fixedly at the corners, and thus the location where the positive and negative vortices meet moves in a restricted way. Fig. 9 shows that the positive vortices separated at the upper corner of the trailing edge move in parallel with the negative vortices which shed slantingly from the lower corner of the leading edge. It is reasonable to deduce that due to the presence of the upper corner of the trailing edge, the positive vortices above the rectangular cylinder forced to reattach the upper surface of the cross-section is restricted from moving downward, leading to the separation of the upper and lower shear layers. Thus, the pairing of vortices is absent and the vortex shedding phenomena disappear. The instantaneous streamlines around rectangular cylinders shown in Fig. 10 demonstrate that large-scale counter-rotating vortices are established behind the trailing edge. For the square, a large portion of the area in the wake is occupied by two counter-rotating vortices which maintain their presence throughout with the strengths rising and falling periodically. For rectangular cylinders with  $w/l$  equal to 2.5 and 3.0, the upper vortical area arises when the lift rises to maximum value but vanishes when the lift lowers back to minimum value. On the other side, the lower vortical area consists of two distinct vortices with one right under the rectangular cylinder and the other behind the trailing edge interacting with the upper vortex. The two patterns of streamline in Fig. 10 reveal two differed patterns of suppressed vortex shedding for the separated and reattached flow, respectively. It is worth noting that the rise and fall of the counter-rotating vortices in the wake result in the periodicity of the flow, which is distinctly different from that of the vortex shedding flows discussed above.

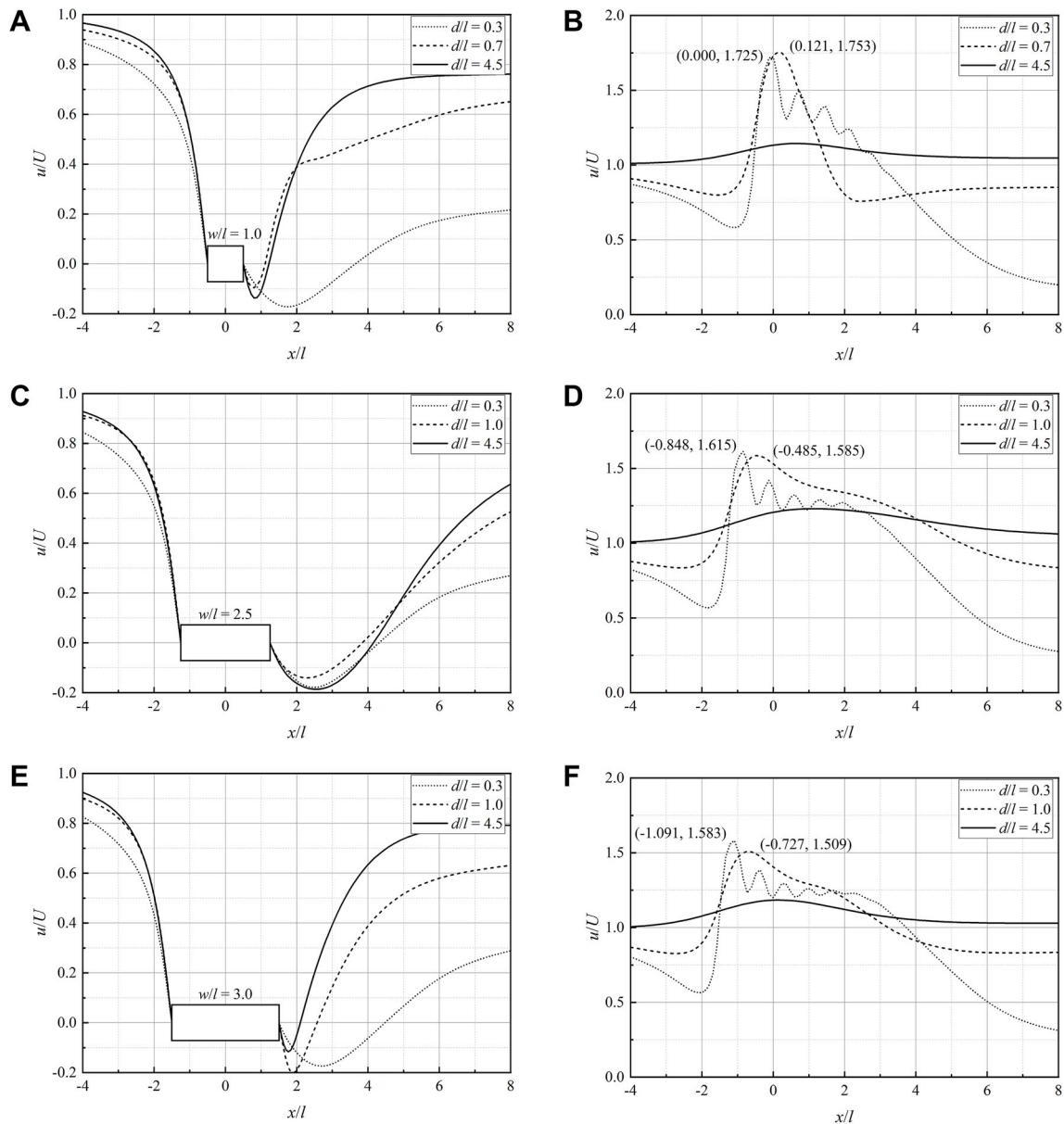
#### 4.4. Discussion on the velocity

Fig. 11(a), (c) and (e) depict the time-averaged streamwise velocity along the centerline of rectangular cylinders with  $w/l$  equal to 1.0, 2.5 and 3.0, respectively. The effect of decreasing  $d/l$  on the velocity upstream of the cylinder is significant only when the asymmetric vortex shedding becomes suppressed as  $d/l$  decreases. By contrast, the velocity downstream of the cylinder varies significantly with  $d/l$ . Particularly, the time-averaged length of the recirculation region changes greatly when  $d/l$  decreases except the cases with  $w/l = 2.5$ . It is also observed that the suppression of vortex shedding leads to the dramatically reduced velocity in the wake. Fig. 11(a), (c) and (e) show that the streamwise velocity downstream of the rectangular cylinder is notably lower than the incoming velocity (lower than half of the incoming velocity). This is due to the large-scale counter-rotating vortices in the wake, causing a low time-averaged value of the velocity.

The velocity above the rectangular cylinder is of interests since the resultant local Froude number,  $Fr (= U/(gd)^{0.5}$ , where  $g$  is the acceleration due to gravity), in the area between the free surface and the cylinder would be significantly larger than the global Froude number. Fig. 11(b), (d) and (f) show the time-averaged streamwise velocity along the centerline of the local area between the free surface and the upper surface of the rectangular cylinder. It is seen that when  $d/l$  is 4.5, the velocity above the rectangular cylinder is roughly equal to the incoming velocity except a slight rise near the top of the cylinder. The slight rise of the velocity is not caused by the free-surface effect but stems from the cylinder which exists to accelerate the surrounding fluid particles in the sense of mass conservation. As the rectangular cylinder approaches the



**Fig. 10.** Instantaneous streamlines around rectangular cylinders with  $w/l$  equal to 1.0, 2.5 and 3.0 located at  $d/l = 0.3$  when the lift is minimum ((a), (c) and (e)) and maximum ((b), (d) and (f)).



**Fig. 11.** Time-averaged streamwise velocity around rectangular cylinders with  $w/l$  equal to 1.0, 2.5 and 3.0 located at different  $d/l$ : (a), (c) and (e) along the centerline of the rectangular cylinder; (b) (d) and (f) along the centerline of the area between the free surface and the upper surface of the rectangular cylinder.

free surface, the velocity above the cylinder increases remarkably. Fig. 11(b) shows that for the rectangular cylinder with  $w/l = 1.0$  located at  $d/l = 0.7$ , the highest velocity reaches about 1.7 times the incoming velocity and occurs at around  $0.6l$  downstream of the leading edge. In contrast, the velocity upstream and downstream of the square decreases jointly to preserve the overall mass conservation. Similar situations apply to rectangular cylinders with  $w/l$  equal to 2.5 and 3.0 located at  $d/l = 1.0$ . Fig. 11(d) and (f) show that the highest velocities reach about 1.5 times the incoming velocity and occur at around  $0.8l$  downstream of the leading edge. It is noted that the flow reattachment of rectangular cylinders with  $w/l = 2.5$  and  $w/l = 3.0$  acts to reduce the highest local velocity and push the position where the highest velocity obtains downstream comparing to the square case. To put it more clearly, the dramatic surface evolution in the asymmetrically separated flow cause higher local velocity while the reduced fluctuations of the surface associated with the one-sidedly or asymmetrically reattached flow contribute to the relatively lower local velocity. Moreover, Fig. 11(d) and (f) show that with the reattachment of the flow, the rate of variation

of the velocity along the centerline of the local area undergoes a sudden change at near the trailing edge. This is due to the interaction of the vortices at the upper corner of the trailing edge accompanying the reattachment of the upper shear layer. As the submersion depth of the rectangular cylinder further decreases, when the vortex shedding is suppressed, the highest velocity varies slightly but the velocity profile changes notably. Fig. 11(b), (d) and (f) show that when  $d/l$  is 0.3, the velocity rises and falls multiple times on top of the cylinder before descending sharply at near the trailing edge. This is believed to be the result of the wave fluctuations of the free surface.

Fig. 12(a) and (b) plot the highest streamwise velocity along the centerline of the area between the free surface and the rectangular cylinder and along the line at the same distance below the cylinder at various  $d/l$ , respectively. It is observed that when  $d/l$  is 4.5, the highest velocity above and under the rectangular cylinder is approximately equal. As  $d/l$  decreases, the highest velocity above the cylinder increases continuously except an unexpected fall from  $d/l = 0.5$  to  $d/l = 0.3$  while the highest velocity under the cylinder increases first and then drops

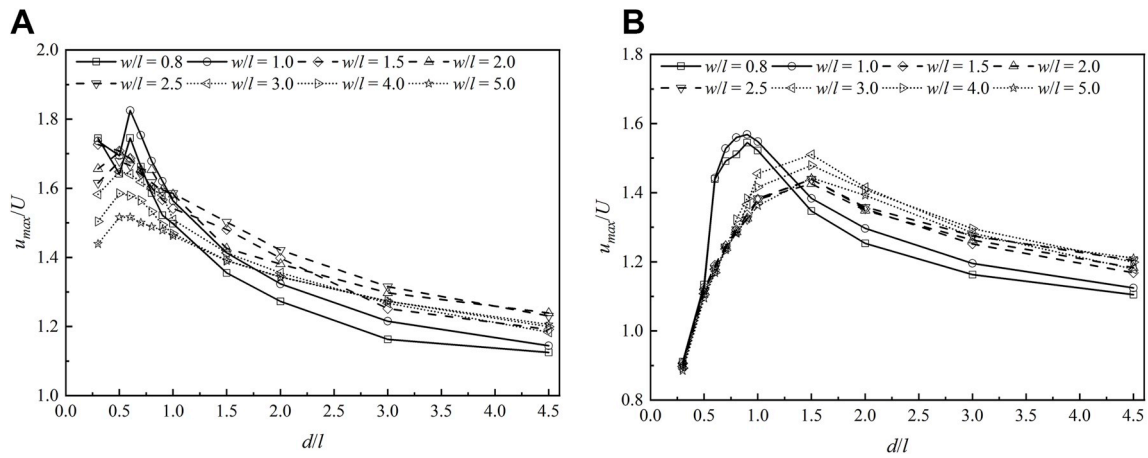


Fig. 12. Effect of  $d/l$  on the highest time-averaged streamwise velocity (a) along the centerline of the area between the free surface and the upper surface of the rectangular cylinder and (b) along the line at the same distance below the cylinder.

dramatically when  $d/l$  is lower than a value. This  $d/l$  value is related to the change of the flow from anti-symmetric to asymmetric as  $d/l$  decreases based on the discussions on the flow structures. Zhong et al. (2019) reported that for rectangular cylinders with  $w/l = 1.0$  and  $w/l = 3.0$ , the free-surface effect becomes significant when  $d/l$  is lower than 1.0. The present study puts it further based on Fig. 12(b) that for rectangular cylinders with  $w/l < 1.5$  and  $w/l \geq 1.5$ , the  $d/l$  ratios, below which the free-surface effect becomes significant, are in the ranges from 0.8 to 1.0 and from 1.0 to 1.5, respectively. This conclusion will be confirmed by the discussions on the force coefficients in the following section. Fig. 12 also illustrates the different variation trends of the highest velocity with  $d/l$  for rectangular cylinders with  $w/l < 1.5$  and  $w/l \geq 1.5$ . This reflects their different variation processes of the

interaction between the free surface and the vortex shedding as  $d/l$  decreases, and highlights the difference between the asymmetrically separated flow and the one-sidedly reattached and asymmetrically reattached flows.

4.5. Discussion on the force coefficients

The behaviors of the force coefficients of rectangular cylinders with  $w/l$  equal to 1.0 and 3.0 under varying  $d/l$  have been analyzed and a close connection between the effects of  $d/l$  and  $w/l$  has been reported by Zhong et al. (2019). In the present paper, a comprehensive analysis of the force coefficients of rectangular cylinders with various  $w/l$  ranging from 0.7 to 5.0 located at different  $d/l$  is conducted.

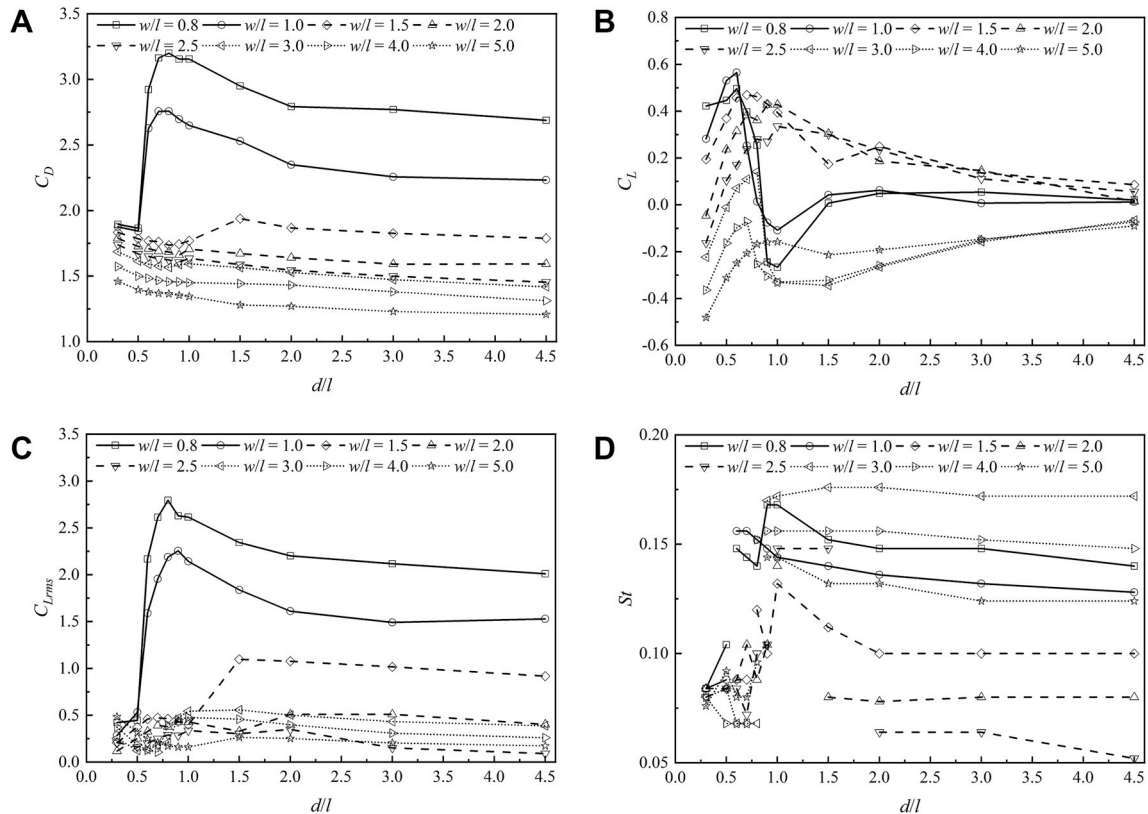


Fig. 13. Time-averaged force coefficients of rectangular cylinders with various  $w/l$  located at different  $d/l$ : (a) Drag coefficient; (b) Lift coefficient; (c) The r.m.s. value of the lift coefficient; (d) Strouhal number.

The drag coefficient of rectangular cylinders located at different  $d/l$  is drawn in Fig. 13(a) when  $w/l$  is 0.8 or 1.0, the drag coefficient varies with  $d/l$  in a similar way, which represents the typical behaviors of the drag coefficient with decreasing  $d/l$  when the separated vortex shedding successively becomes asymmetric and suppressed. Specifically, the rise of the drag coefficient from  $d/l = 4.5$  to around  $d/l = 0.8$  reflects the process in which the interaction between the free surface and the separated flow becomes significant and the low drag coefficient at  $d/l \leq 0.5$  implies the occurrence of the suppressed vortex shedding. The maximum drag coefficient of rectangular cylinders with  $w/l$  equal to 0.8 and 1.0 occurs at around  $d/l = 0.8$ , which marks the beginning of the asymmetric vortex shedding as  $d/l$  decreases. When  $w/l$  is 3.0, 4.0 and 5.0, the drag coefficient also varies similarly with  $d/l$ . This variation of the drag coefficient corresponds to the change of the reattached flow when approaching a free surface. The maximum drag coefficient for rectangular cylinders with  $w/l > 2.8$  is predicted to be obtained in the extreme case of  $d = 0$ , which is consistent with Zhong et al. (2019). It is found that the variation trends of the drag coefficient with  $d/l$  in the two  $w/l$  ranges are basically similar although the amplitudes of variation and the corresponding  $d/l$  ranges are different. These differences are apparently attributed to the different patterns of interaction between the free surface and the cylinder. For rectangular cylinders with  $w/l$  between 1.5 and 2.8, the variations of the drag coefficient with  $d/l$  are generally in resemblance to the cases with  $w/l > 2.8$ . The cause for this is the one-sided reattachment of the flow when the cylinder approaches the free surface.

The three patterns of flow variations associated with the three  $w/l$  ranges are also reflected in the variations of the lift coefficient. Fig. 13(b) clearly shows three distinct variation trends of the lift coefficient with  $d/l$ . Importantly, the lift coefficient varies remarkably in the  $d/l$  range from 1.0 to 0.3. The sharp rise of the lift coefficient begins at around  $d/l = 0.9$  and ends at  $d/l = 0.6$  when  $w/l$  is 0.8 or 1.0, while when  $w/l$  is larger than 2.8, the lift coefficient starts rising at  $d/l = 1.0$  or 1.5 and peaks at around  $d/l = 0.8$ . For rectangular cylinders with  $1.5 \leq w/l < 2.8$ , the lift coefficient decreases sharply from around  $d/l = 0.9$  to  $d/l = 0.3$ . The  $d/l$ , at which the lift coefficient starts varying dramatically, is also reflected in the variations of the r.m.s. value of the lift coefficient as shown in Fig. 13(c), and is consistent with the variations of the local velocity under the rectangular cylinder (see Fig. 12(b)). These  $d/l$  are regarded as important values, below which the free-surface effect becomes significant, and can be used to define the boundary between the anti-symmetric flow and the asymmetric flow.

Fig. 13(d) indicates that when  $w/l$  is within  $0.7 \leq w/l < 1.5$  and  $w/l > 2.8$ , the Strouhal number is of the same order of magnitude as the infinite-medium cases and increases as  $d/l$  decreases from 4.5 to a critical value. For example, when  $w/l$  is 0.8 or 1.0, the Strouhal number rises generally as  $d/l$  decreases from 4.5 to 0.6, which is consistent with the discussions on the vortex shedding frequency in Fig. 6. When  $w/l$  falls between 1.5 and 2.8, due to the occurrence of the one-sided flow reattachment, the Strouhal number rises suddenly at some  $d/l$  ratio. As shown by the dashed lines representing  $w/l = 1.5$ ,  $w/l = 2.0$  and  $w/l = 2.5$  in Fig. 13(d), the sharp rise of the Strouhal number occurs at  $d/l = 1.5$  or  $d/l = 2.0$  depending on  $w/l$ . In addition, it is observed that for all the cases, when  $d/l$  decreases passing a critical value, the Strouhal number drops sharply. The low Strouhal number at low  $d/l$  reflects the low flow period which is the typical characteristic of the suppressed vortex shedding. Recently, Zhong et al. (2019) reported the critical  $d/l$  values for rectangular cylinders with  $w/l$  equal to 1.0 and 3.0. In the present study, a general relationship between the critical  $d/l$  and  $w/l$  is given. Fig. 13(d) demonstrates that the critical  $d/l$  for rectangular cylinders with  $w/l$  in the ranges from 0.7 to 1.5 and from 2.8 to 5.0 are in the ranges from 0.5 to 0.6 and from 0.8 to 0.9, respectively. The critical  $d/l$  for rectangular cylinders with  $w/l$  between 1.5 and 2.8 varies slightly as  $w/l$  increases and is located between 0.7 and 1.0.

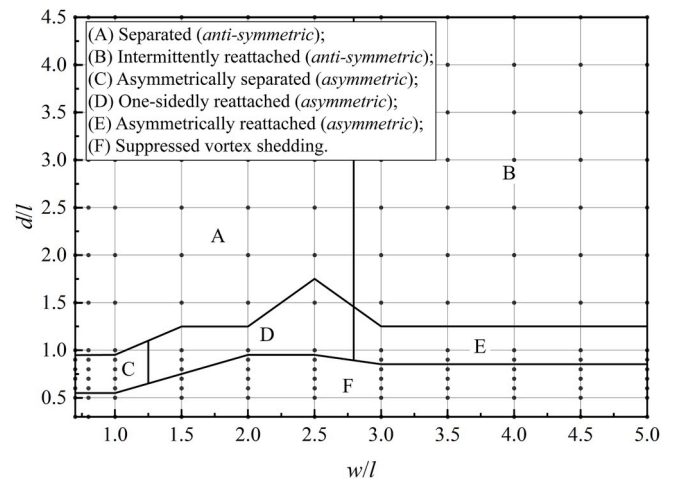


Fig. 14. Boundaries between different flow patterns in the  $w/l - d/l$  space.

#### 4.6. Boundaries between different flow patterns

Based on the above discussions, it is clear that there is a close relation between the change of the flow and the variations of the force coefficients with  $d/l$ . Therefore, it is possible that the boundaries between different flow patterns can be defined based on the behaviors of the force coefficients under varying  $d/l$ . The boundaries between different flow patterns for rectangular cylinders with various  $w/l$  approaching a free surface are given in Fig. 14. The criteria for defining the boundaries are as follows:

- The boundary between the anti-symmetric flow and the asymmetric flow depends on the pattern of the asymmetric flow. When the asymmetric flow is asymmetrically separated or asymmetrically reattached, since there is no substantial rise of the Strouhal number with decreasing  $d/l$ , the boundary is selected as the  $d/l$  value, at which the lift coefficient starts rising as  $d/l$  decreases. When the asymmetric flow is one-sidedly reattached, the  $d/l$ , at which the Strouhal number jumps abruptly as  $d/l$  decreases, is selected to be the boundary.
- The boundary between the asymmetric flow and the suppressed vortex shedding is defined as the critical  $d/l$ , below which the Strouhal number drops suddenly.

Fig. 14 shows that the  $d/l$ , above which the flow is anti-symmetric, depends on  $w/l$ . It is observed that when  $d/l$  is larger than 1.5, the interaction between the free surface and rectangular cylinders with  $w/l$  between 0.7 and 5.0 is insignificant. The  $d/l$  range, over which the asymmetric flow displays, is small comparing to that of the anti-symmetric flow. The flow rapidly becomes dominated by the free-surface effect as  $d/l$  decreases and the critical  $d/l$  is dependent on  $w/l$ . It is revealed by Fig. 14 that the critical  $d/l$  for the reattached flow is larger than that of the separated flow. Specifically, for rectangular cylinders with  $0.7 \leq w/l < 1.5$  and  $w/l > 2.8$ , the critical  $d/l$  falls within the ranges from 0.5 to 0.6 and from 0.8 to 0.9, respectively. For rectangular cylinders with  $1.5 \leq w/l < 2.8$ , the critical  $d/l$  varies slightly with  $w/l$  and is located between 0.7 and 1.0. It is preferable to avoid placing the rectangular cylinder lower than the critical  $d/l$  value, since a large portion of the wake is occupied by the large-scale counter-rotating vortices which may cause adverse impacts on surrounding structural components. A research on the flow around rectangular cylinders in a tandem arrangement close to a free surface is needed in order to understand the phenomena.

## 5. Concluding remarks

Flow past rectangular cylinders in the vicinity of a free surface was investigated in the present study. Two-dimensional simulations were conducted using the Mentor SST  $k - \omega$  model and the VoF method. The flow structures, velocity field and force coefficients of rectangular cylinders with  $w/l$  between 0.7 and 5.0 located at different  $d/l$  ranging from 0.3 to 4.5 were analyzed. The following conclusions were drawn:

1. The flow around a deeply submerged rectangular cylinder is anti-symmetric, which is similar to that in an infinite-medium case. When the rectangular cylinder approaches a free surface, the flow becomes asymmetric due to the one-sided constraint from the surface. There are three patterns of asymmetric flow depending on  $w/l$ : “asymmetrically separated”, “one-sidedly reattached” and “asymmetrically reattached”. The asymmetrically separated flow appears around rectangular cylinders with low  $w/l$ , i.e.,  $w/l < 1.5$ , and is characterized by the separation of the flow even under the effect of the free surface. When  $w/l$  is between 1.5 and 2.8, the upper shear layer is reattached onto the upper surface of the cylinder while the lower shear layer is detached, causing the one-sidedly reattached flow. When  $w/l$  is larger than 2.8, the reattached flow displayed at deep depths becomes asymmetrically reattached when the rectangular cylinder approaches the free surface, with the reattaching points on the upper and lower surfaces moving upstream and downstream respectively.
2. The vortex shedding around rectangular cylinders becomes suppressed when  $d/l$  is low, and consequently, large-scale counter-rotating vortices are established in the wake. There are two patterns of streamline for the suppressed vortex shedding. One is featured by two counter-rotating vortices which maintain their presence throughout with the strengths rising and falling periodically. The other is featured by the upper periodically arising vortex and the lower vortical area which consists of two vortices under the cross-section and behind the trailing edge respectively. The two streamline patterns reveal two differed patterns of suppressed vortex shedding for the separated and reattached flow, respectively.
3. The streamline velocity downstream of the rectangular cylinder varies dramatically as  $d/l$  decreases, especially when the vortex shedding is suppressed. With the suppression of vortex shedding, the velocity in the wake is notably lower than the incoming velocity due to the large-scale counter-rotating vortices. Moreover, the velocity above the rectangular cylinder rises remarkably higher than the incoming velocity as  $d/l$  decreases, leading to a local high Froude number. Variations of the local velocity with  $d/l$  provide a mean to distinguish the different flow patterns.
4. The behaviors of the force coefficients of rectangular cylinders with  $w/l$  in the ranges of  $0.7 < w/l < 1.5$ ,  $1.5 \leq w/l < 2.8$  and  $2.8 < w/l \leq 5.0$  under varying  $d/l$  show different characteristics due to the different patterns of flow variations associated with the three  $w/l$  ranges. The maximum drag coefficient occurs at around  $d/l = 0.8$  when  $w/l$  is lower than 1.5, while the maximum drag coefficient for rectangular cylinders with  $w/l \geq 1.5$  is predicted to be obtained in the extreme case of  $d = 0$ . The lift coefficient varies dramatically in the  $d/l$  range from 1.0 to 0.3 corresponding to the change of the flow from asymmetric to suppressed. The low Strouhal number appearing at low  $d/l$  indicates the occurrence of the suppressed vortex shedding.
5. The boundaries between different flow patterns were defined based on the variations of the force coefficients with  $d/l$ . When  $d/l$  is larger than 1.5, the interaction between the free surface and rectangular cylinders with  $w/l$  between 0.7 and 5.0 is insignificant. The critical  $d/l$ , below which the vortex shedding is suppressed, falls within the ranges from 0.5 to 0.6 and from 0.8 to 0.9 for rectangular cylinders with  $0.7 \leq w/l < 1.5$  and  $w/l > 2.8$ , respectively. The critical  $d/l$  for

rectangular cylinders with  $1.5 \leq w/l < 2.8$  varies slightly with  $w/l$  and is located between 0.7 and 1.0.

## Declaration of competing interest

The authors declare that they have no known competing financial interests or personal relationships that could have appeared to influence the work reported in this paper.

## CRediT authorship contribution statement

**Wenjie Zhong:** Conceptualization, Methodology, Software, Validation, Writing - original draft, Visualization. **Solomon C. Yim:** Resources, Writing - review & editing, Supervision, Project administration. **Lu Deng:** Writing - review & editing, Supervision, Project administration, Funding acquisition.

## Acknowledgement

This work has been supported by National Natural Science Foundation of China (grant NO. 51778222) and China Scholarship Council (grant NO. 201806130143). These supports are gratefully acknowledged. The first and second authors also acknowledge the support from the School of Civil and Construction Engineering at Oregon State University where the first author is a visiting doctorate student.

## Appendix A. Supplementary data

Supplementary data to this article can be found online at <https://doi.org/10.1016/j.oceaneng.2020.107049>.

## References

- Angrilli, F., Bergamaschi, S., Cossalter, V., 1982. Investigation of wall induced modifications to vortex shedding from a circular cylinder. *J. Fluid Eng.* 104 (4), 518–522.
- Bearman, P.W., Obasaju, E.D., 1982. An experimental study of pressure fluctuations on fixed and oscillating square-section cylinders. *J. Fluid Mech.* 119, 297–321.
- Bosch, G., Kappler, M., Rodi, W., 1996. Experiments on the flow past a square cylinder placed near a wall. *Exp. Therm. Fluid Sci.* 13 (3), 292–305.
- Bovand, M., Rashidi, S., Esfahani, J.A., Masoodi, R., 2016. Control of wake destructive behavior for different bluff bodies in channel flow by magnetohydrodynamics. *Eur. Phys. J. Plus* 131 (6), 194.
- Bruinsma, N., Paulsen, B.T., Jacobsen, N.G., 2018. Validation and application of a fully nonlinear numerical wave tank for simulating floating offshore wind turbines. *Ocean. Eng.* 147, 647–658.
- Durao, D.F.G., Heitor, M.V., Pereira, J.C.F., 1988. Measurements of turbulent and periodic flows around a square cross-section cylinder. *Exp. Fluid* 6 (5), 298–304.
- Farhadi, M., Rahnama, M., 2005. Three-dimensional study of separated flow over a square cylinder by large eddy simulation. *Proc. IME G J. Aero. Eng.* 219, 225–234.
- Goktun, S., 1975. The Drag and Lift Characteristics of a Cylinder Placed Near a Plane Surface, Master's Thesis. Naval Postgraduate School, Monterey, California, USA.
- Higuera, P., Lara, J.L., Losada, I.J., 2013a. Realistic wave generation and active wave absorption for Navier–Stokes models: application to OpenFOAM®. *Coast. Eng.* 71, 102–118.
- Higuera, P., Lara, J.L., Losada, I.J., 2013b. Simulating coastal engineering processes with OpenFOAM®. *Coast. Eng.* 71, 119–134.
- Hirt, C.W., Nichols, B.D., 1981. Volume of fluid (VOF) method for the dynamics of free boundaries. *J. Comput. Phys.* 39 (1), 201–225.
- Holzmann, T., 2016. Mathematics, numerics, derivations and OpenFOAM®, Loeben, Germany: Holzmann CFD (visited on Nov. 29, 2017). <https://holzmann-cfd.de>.
- Hu, Z.Z., Greaves, D., Raby, A., 2016. Numerical wave tank study of extreme waves and wave-structure interaction using OpenFOAM®. *Ocean. Eng.* 126, 329–342.
- Jacobsen, N.G., Fuhrman, D.R., Fredsøe, J., 2012. A wave generation toolbox for the open-source CFD library: OpenFoam®. *Int. J. Numer. Methods Fluid.* 70 (9), 1073–1088.
- Lee, B.E., 1975. The effect of turbulence on the surface pressure field of a square prism. *J. Fluid Mech.* 69, 263–282.
- Lei, C., Cheng, L., Armfield, S.W., Kavanagh, K., 2000. Vortex shedding suppression for flow over a circular cylinder near a plane boundary. *Ocean. Eng.* 27 (10), 1109–1127.
- Liu, I.H., Righlin, J., Schleicher, W.C., Oztekin, A., 2016. Flow past a plate in the vicinity of a free surface. *Ocean. Eng.* 111, 323–334.
- Lyn, D.A., Einav, S., Rodi, W., Park, J.H., 1995. A laser-Doppler velocimetry study of ensemble-averaged characteristics of the turbulent near wake of a square cylinder. *J. Fluid Mech.* 304, 285–319.

- Machado, F.M.M., Lopes, A.M.G., Ferreira, A.D., 2018. Numerical simulation of regular waves: optimization of a numerical wave tank. *Ocean. Eng.* 170, 89–99.
- Malavasi, S., Guadagnini, A., 2003. Hydrodynamic loading on river bridges. *J. Hydraul. Eng. Asce* 129 (11), 854–861.
- Malavasi, S., Guadagnini, A., 2007. Interactions between a rectangular cylinder and a free-surface flow. *J. Fluid Struct.* 23 (8), 1137–1148.
- Mannini, C., Soda, A., Schewe, G., 2010. Unsteady RANS modelling of flow past a rectangular cylinder: investigation of Reynolds number effects. *Comput. Fluid* 39 (9), 1609–1624.
- Martínez-Ferrer, P.J., Qian, L., Ma, Z., Causon, D.M., Mingham, C.G., 2018. Improved numerical wave generation for modelling ocean and coastal engineering problems. *Ocean. Eng.* 152, 257–272.
- Martinuzzi, R.J., Bailey, S.C.C., Kopp, G.A., 2003. Influence of wall proximity on vortex shedding from a square cylinder. *Exp. Fluid* 34 (5), 585–596.
- Menter, F.R., 1994. Two-equation eddy-viscosity turbulence models for engineering applications. *AIAA J.* 32 (8), 1598–1605.
- Miyata, H., Shikazono, N., Kanai, M., 1990. Forces on a circular cylinder advancing steadily beneath the free-surface. *Ocean. Eng.* 17 (1), 81–104.
- Moukalled, F., Mangani, L., Darwish, M., 2015. *The Finite Volume Method in Computational Fluid Dynamics: an Advanced Introduction with OpenFOAM and Matlab*. Springer Publishing Company, Incorporated.
- Nakaguchi, H., Hashimoto, K., Muto, S., 1968. An experimental study on aerodynamic drag of rectangular cylinders. *J. Jpn. Soc. Aeronaut. Space Sci.* 16 (168), 1–5.
- Norberg, C., 1993. Flow around rectangular cylinders: pressure forces and wake frequencies. *J. Wind Eng. Ind. Aerod.* 49 (1–3), 187–196.
- Ohtsuki, Y., 1978. Wind tunnel experiments on aerodynamic forces and pressure distributions of rectangular cylinders in a uniform flow. *Proc. 5th Symp. Wind Eff. Struct.* 169–175.
- Okajima, A., 1982. Strouhal numbers of rectangular cylinders. *J. Fluid Mech.* 123, 379–398.
- Ong, M.C., Utnes, T., Holmedal, L.E., Myrhaug, D., Pettersen, B., 2009. Numerical simulation of flow around a smooth circular cylinder at very high Reynolds numbers. *Mar. Struct.* 22 (2), 142–153.
- Price, S.J., Sumner, D., Smith, J.G., Leong, K., Paidoussis, M.P., 2002. Flow visualization around a circular cylinder near to a plane wall. *J. Fluid Struct.* 16 (2), 175–191.
- Rashidi, S., Bovand, M., Esfahani, J.A., Öztöp, H.F., Masoodi, R., 2015. Control of wake structure behind a square cylinder by magnetohydrodynamics. *J. Fluid Eng.* 137 (6), 061102.
- Rashidi, S., Bovand, M., Esfahani, J.A., 2016a. Application of magnetohydrodynamics for suppressing the fluctuations in the unsteady flow around two side-by-side circular obstacles. *Eur. Phys. J. Plus* 131 (12), 423.
- Rashidi, S., Esfahani, J.A., 2015. The effect of magnetic field on instabilities of heat transfer from an obstacle in a channel. *J. Magn. Magn. Mater.* 391, 5–11.
- Rashidi, S., Hayatdavoodi, M., Esfahani, J.A., 2016b. Vortex shedding suppression and wake control: a review. *Ocean. Eng.* 126, 57–80.
- Reichl, P., Hourigan, K., Thompson, M.C., 2005. Flow past a cylinder close to a free surface. *J. Fluid Mech.* 533, 269–296.
- Rusche, H., 2003. *Computational Fluid Dynamics of Dispersed Two-phase Flows at High Phase Fractions*. Doctoral dissertation. Imperial College London (University of London).
- Schewe, G., 2013. Reynolds-number-effects in flow around a rectangular cylinder with aspect ratio 1:5. *J. Fluid Struct.* 39 (5), 15–26.
- Sheridan, J., Lin, J.C., Rockwell, D., 1995. Metastable states of a cylinder wake adjacent to a free surface. *Phys. Fluids* 7 (9), 2099–2101.
- Sheridan, J., Lin, J.C., Rockwell, D., 1997. Flow past a cylinder close to a free surface. *J. Fluid Mech.* 330, 1–30.
- Shimada, K., Ishihara, T., 2002. Application of a modified  $k - \epsilon$  model to the prediction of aerodynamic characteristics of rectangular cross-section cylinders. *J. Fluid Struct.* 16 (4), 465–485.
- Sohankar, A., 2006. Flow over a bluff body from moderate to high Reynolds numbers using large eddy simulation. *Comput. Fluid* 35 (10), 1154–1168.
- Sohankar, A., 2008. Large eddy simulation of flow past rectangular-section cylinders: side ratio effects. *J. Wind Eng. Ind. Aerod.* 96 (5), 640–655.
- Stringer, R.M., Zang, J., Hillis, A.J., 2014. Unsteady RANS computations of flow around a circular cylinder for a wide range of Reynolds numbers. *Ocean. Eng.* 87 (5), 1–9.
- Tian, X.L., Ong, M.C., Yang, J.M., Myrhaug, D., 2013. Unsteady RANS simulations of flow around rectangular cylinders with different aspect ratios. *Ocean. Eng.* 58 (58), 208–216.
- Ubbink, O., 1997. *Numerical Prediction of Two Fluid Systems with Sharp Interfaces*. Imperial College.
- Wang, X.K., Tan, S.K., 2008. Comparison of flow patterns in the near wake of a circular cylinder and a square cylinder placed near a plane wall. *Ocean. Eng.* 35 (5–6), 458–472.
- Zhong, W., Deng, L., Xiao, Z., 2019. Flow past a rectangular cylinder close to a free surface. *Ocean. Eng.* 186, 106118.